Journal of Power Sources 687 (2026) 240526

Contents lists available at ScienceDirect

Journal of Power Sources

journal homepage: www.elsevier.com/locate/jpowsour

Review article

Advancement and growth of metal organic framework derived nanostructured materials for fabrication of high energy density supercapacitors

P. Varatharajan [a], Kumar Gokulkumar [a], Shih-Hsuan Chen [a], Neeraja Bose [a], Elango Kandasamy [b,c,*], Kun-Mu Lee [a,d,e,f,**]

[a] Center for Sustainability and Energy Technologies, Chang Gung University, Taoyuan, 33302, Taiwan
[b] Department of Chemistry, Amrita School of Physical Sciences, Amrita Vishwa Vidyapeetham, Coimbatore, India
[c] Functional Materials Laboratory, Amrita School of Engineering, Amrita Vishwa Vidyapeetham, Coimbatore, India
[d] Department of Chemical and Materials Engineering, Chang Gung University, Taoyuan, 33302, Taiwan
[e] Division of Neonatology, Department of Pediatrics, Chang Gung Memorial Hospital, Linkou, Taoyuan, 33305, Taiwan
[f] College of Environment and Resources, Ming Chi University of Technology, New Taipei City, 24301, Taiwan

HIGHLIGHTS

- MOF derived materials are critically reviewed for high energy density SCs.
- Synthesis routes and key physicochemical properties are systematically summarized.
- Electrochemical performance of MOF derived electrodes is comparatively discussed.
- Theoretical and in situ/operando analyses are integrated for mechanistic insight.
- Limitations and commercialization prospects for MOF derived electrodes are outlined.

ARTICLE INFO

Keywords:
Supercapacitor
MOF derived nanostructure
Transition metal components
Heterostructure
High energy density

ABSTRACT

Over the past two decades, metal organic frameworks (MOFs) has proven to be highly adaptable porous materials for energy related applications due to their exceptional surface area, tunable pore structure and structural diversity. Beyond their intrinsic properties, MOFs be employed as effective sacrificial templates for deriving transition metal oxides (TMOs), sulfides, phosphates, hydroxides, porous carbon, and their heterostructured composites. These MOF derived nanostructured materials are appealing for high energy density supercapacitors because they show superior electrochemical performance through increased conductivity, a large number of active sites, and optimized ion transport routes. This review critically summarizes latest advancements in MOF derived nanostructured electrode materials, focusing on the relationship between structural evolution, morphology control, and electrochemical charge storage behaviour. We also discussed about different synthesis condition changes and how they affect physicochemical characteristics. Current challenges, including structural stability, scalable synthesis and device integration are highlighted along with future perspectives for developing advanced electrode materials for modern energy storage technologies.

1. Introduction

The depletion of fossil fuels and the increasing level of environmental pollution driven people to think toward a sustainable energy resources. Recently, government policies have also shifted their focus toward decarbonization to move the country toward zero carbon emissions. This shift has resulted in a significant increase in the use of small electronic gadgets and high-power hybrid electric vehicles.

* Corresponding author. Department of Chemistry, Amrita School of Physical Sciences, Coimbatore, Amrita Vishwa Vidyapeetham, India.
** Corresponding author. Department of Chemical and Materials Engineering, Chang Gung University, Taoyuan, 33302, Taiwan.
E-mail addresses: k_elango@cb.amrita.edu (E. Kandasamy), kmlee@mail.cgu.edu.tw (K.-M. Lee).

https://doi.org/10.1016/j.jpowsour.2026.240526
Received 7 April 2026; Received in revised form 14 May 2026; Accepted 25 May 2026
Available online 4 June 2026

Consequently, the global adoption of electric vehicles necessitates the emergence of energy storage devices with enamours energy density (E_D), and excellent cycle stability [1–3]. Various research teams around the world are working on different components to develop advanced and sustainable energy storage systems. At this stage, supercapacitors (SCs) have come into the spotlight and have attracted notable attention as practical energy storage devices. They possess several unquestionable advantages, such as fast charge–discharge capability, excellent power density (P_D) (>1000 W/kg), appreciable E_D (>5 Wh/kg), and good cycle stability (>10^5 cycles). These characteristics positioned SCs between conventional electrostatic capacitors and batteries [4,5]. Depends on charge storage mechanism of SCs are largely classified into three types such as (i) Electric double layer capacitor (EDLC), (ii) pesudocapacitor (PCs) and (iii) Hybrid supercapacitor (HSC) (Fig. 1). In EDLC based SCs, charge storage follows a non-Faradaic mechanism. During the charging and discharging processes, electrolyte ions are reversibly accumulated and released at the electrode surface without involving any chemical reactions. As a result, EDLC-based SCs demonstrate high charge–discharge rates, excellent cycling stability, and superior P_D. However, it exhibits lower E_D due to the physical charge storage mechanism. The carbon based materials such as activated carbon (AC), graphene, graphene oxide (GO), reduced graphene oxide (rGO) and carbon nanotubes (CNTs) are majorly follows EDLC based behaviour [6]. Pseudocapacitors operate through constant and reversible redox reactions at the electrode surface during charging and discharging cycles. In pseudocapacitors, redox reactions take place on and close to the electrode surface, enabling greater charge storage and thereby achieving high specific capacitance (C_s) and E_D. However, the continuous redox reactions in pseudocapacitors can affect their electrochemical stability over prolonged cycling. Most conducting polymers and transition metal oxides (TMOs) exhibit pseudocapacitive behaviour [7]. Hybrid supercapacitors (HSCs) merge the features of both types, offering enhanced E_D with minimal loss in P_D [8].

Although SCs offer many advantages, commercial SCs still suffer from a major drawback of low energy density, typically ranging from 5 to 8 Wh/kg, which limits their suitability for long-duration energy storage applications. Transition metal oxides (TMOs), such as RuO_2, Co_3O_4, NiO, and MnO_2, can be synthesized through relatively simple methods and can deliver moderate to high energy densities, generally in the range of 5-40 Wh/kg. However, only a limited number of TMO-based SCs have been commercialized so far. This is mainly due to the bulk and aggregated morphologies commonly obtained through traditional synthesis approaches, the difficulty in precisely controlling pore size and pore volume, limited electrical conductivity, and inadequate cycling stability compared with carbon-based SCs. These limitations restrict the practical electrochemical performance and commercial viability of TMO-based supercapacitors. Therefore, significant research efforts have been devoted to the development of metal organic framework (MOF) derived hybrid nanomaterial based electrodes, including ternary TMOs, hydroxides, sulfides, phosphates, porous carbons, and their composites, for high-performance SC devices. These materials are attractive owing to their tailored nanoarchitectures, tunable porosity, enhanced structural stability, and excellent energy density [9–11]. Therefore, the development of such advanced synthesis approaches is crucial for engineering SC electrodes with controlled nanoarchitectures, shortened ion-transport pathways, and enhanced electron-transfer kinetics. These features collectively improve charge-storage efficiency and energy-density performance, thereby helping to narrow the energy-density gap between SCs and commercial Li-ion batteries, which generally deliver energy densities exceeding 150 Wh/kg [12].

MOFs are exemplary crystalline structures composed of inorganic nodes linked by organic connectors via coordination bonds [13]. They are used as core material for multifunctional applications such as energy storage, sensing, removal of environmental contaminants, photo and electrocatalysis [14]. By changing the reaction conditions, solvent environment, and incorporating different metals and organic linkers, their morphological characteristics, pore size, pore volume, and surface area can be effectively tuned. However, the poor electrical conductivity of MOFs due to insulating organic linkers and a lack of redox-active sites limits their efficacy as electrode materials in electrochemical energy storage systems [15]. To overcome this limitation, MOFs are nowadays widely used as excellent sacrificial templates for the fabrication of various nanostructured materials [16]. The MOFs prepared using organic linker series such as 1,3,5-benzenetricarboxylate (BTC) [4,17]-benzenedicarboxylate (BDC) [18] and Zeolite Imidazole Framework (ZIF) [19] are commonly used as an organic linkers for the preparation of MOF and they are most often synthesized by hydrothermal [20], solvothermal [21] and chemical reduction methods [22]. These methods provide simple routes for the preparation of MOFs with uniform morphology and very high specific surface area [23].

The direct and controlled heating of MOFs at high temperature produces a various MOF derived nanostructured material with good composition and morphology. During the heating process, the organic linkers present in MOFs decompose and release CO_2, CO, water vapor, and other volatile compounds, while the transition metal nodes react with oxygen in the atmosphere to form TMOs (Fig. 2). Similarly, sulfurization and phosphorization treatments can convert these metal species into metal sulfides and phosphates, whereas metal hydroxides can be prepared through a direct chemical etching process [24–28]. With that, MOF-derived carbon and their combined metal oxides [29], phosphates [30], sulfides [31], and selenides [32] based nanomaterials also prepared by similar approaches. The nanostructured materials derived from MOFs possess unique morphological features and improved surface area and porosity relative to those prepared using conventional approaches (Fig. 3) [14].

Further, the MOF-on-MOF approach is often used to construct hybrid

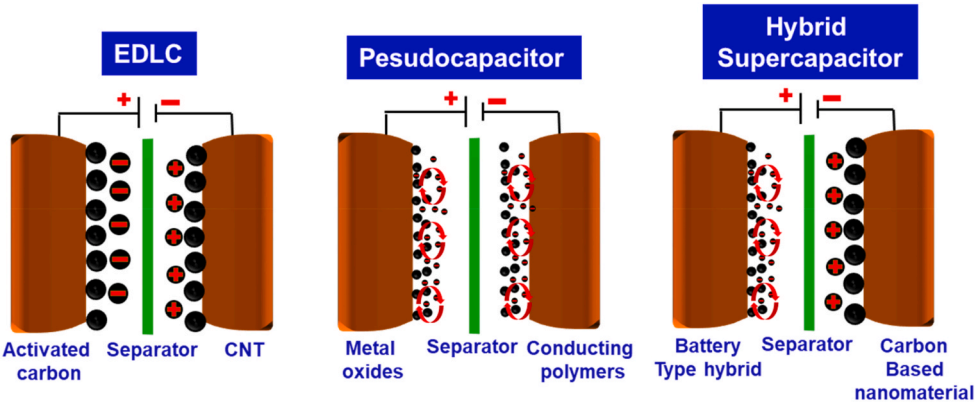

Fig. 1. Different charge storage mechanism of SC.

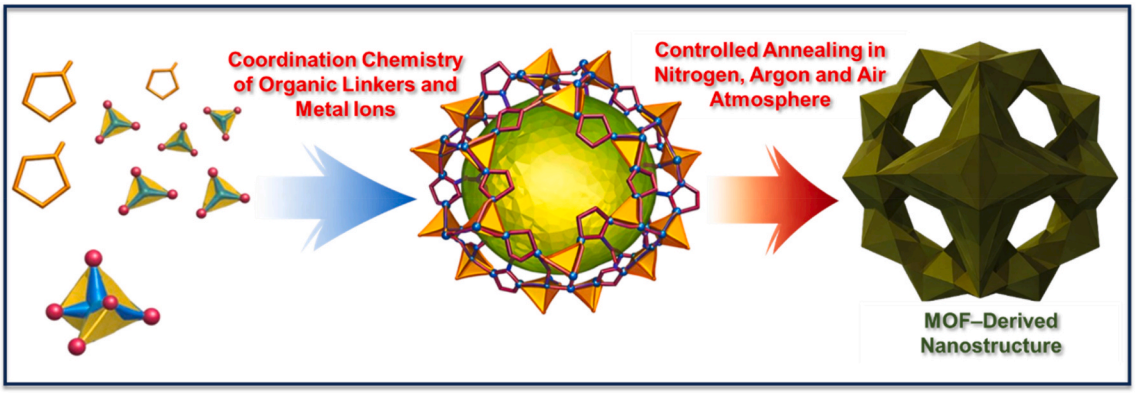

Fig. 2. Diagrammatic illustration of the porous MOF derived nanostructure formation process.

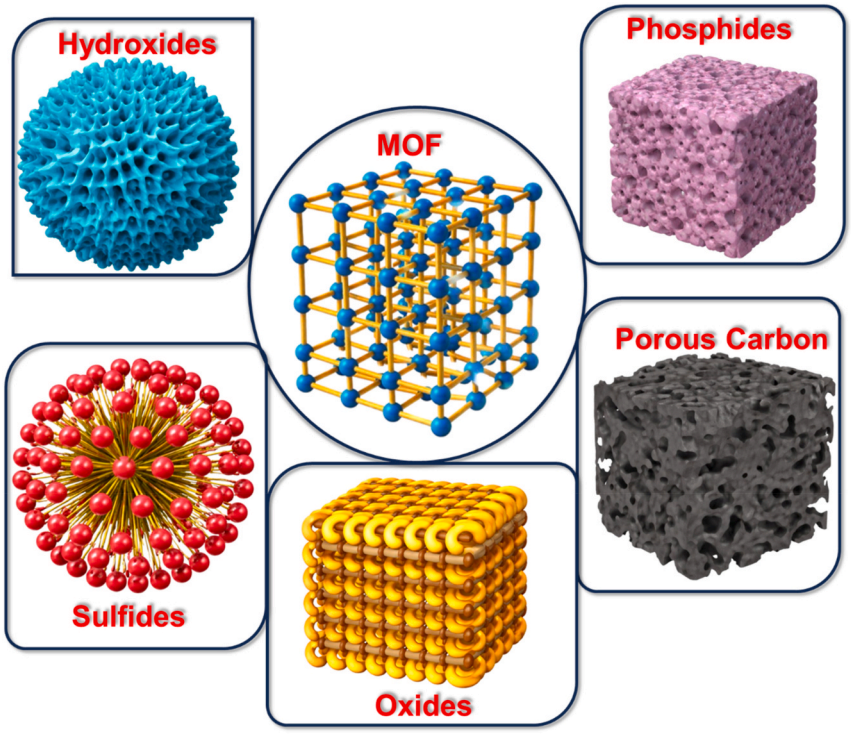

Fig. 3. Schematic representation of MOF derived oxides, hydroxide, phosphides, sulfides and PC.

MOF structures composed of two different MOFs, which are subsequently employed as templates for the synthesis of nanostructured materials. Honglong Qu and his co-workers employed a MOF-on-MOF strategy to synthesize a Ni-MOF/Prussian blue analogue (PBA) hybrid on the surface of Ni-foam (NF) by hydrothermal approach then through phosphorization $Co_2P/Ni_2P/NF$ synthesized [33]. Furthermore, carbonization of MOFs in a fully inert environment can create high-quality porous carbon (PC) with uniform porosity and high specific surface area (~3000 $m^2\,g^{-1}$). This method is simple and facile, enabling the production of multidimensional PC through a one-step carbonization approach. The metal ions present on the PC surface are subsequently removed by chemical etching [34,35]. Additionally, doping with different heteroatoms such as fluorine (F), sulfur (S), nitrogen (N), and phosphorus (P) and alkaline based activation technique can further enhance the redox active sites, surface defects and electrical conductivity of PC which significantly strengthen their electrochemical characteristics [36]. Furthermore, hybridization of MOF derived nanomaterials with various carbon based materials, such as CNTs [37], CNFs [38], GO [39], and rGO [40], are widely employed to improve conductivity and structural stability. These diverse properties, abundant options for electrode modification, unique morphologies, and the presence of essential redox-active sites make MOF-derived nanostructures and composite materials among the most promising candidates for SC applications.

Previous reviews in this field have mainly looked at improving material design and capacitance but energy density oriented device performance in MOF-derived systems remains limited. This review provides a comprehensive overview of recent advancements in MOF derived nanostructured materials and their composites for high energy density SCs, with a focus on studies since 2021 reporting device-level energy density (E_D > 20 Wh/kg). MOF-derived metal oxides, phosphates, sulfides, PC, and their composites synthesis, structural, electrochemical characteristics and various energy storage parameters in different conditions are discussed in detail with separate sections, and a comparative table is provided to summarize the reported results. The challenges and future strategies for improving electrode material architecture to achieve high energy density SC and strategies enable commercialization of SC are also discussed.

2. MOF derived nanostructured materials for SC application

MOF derived approach through chemical and thermal processes provide ample opportunities for researchers to fabricate nanostructured materials with novel chemical compositions, large specific surface area, unique morphologies and high porosity. These properties are highly desirable for electrode materials used in SCs. Over the last five years, researchers have achieved significant improvements in high E_D and prominent cycle stability in SC devices with the help of nanostructured materials derived from MOF.

2.1. MOF derived single, binary and ternary TMOs and their composites for SC application

Electrodes are critical components of SC devices that influence overall device performance. TMOs, especially NiO, Co_3O_4, Fe_2O_3, MnO_2, RuO_2, various mixed TMOs, and their composites, are regarded as effective pseudocapacitive electrode materials. Due to their reversible faradaic behaviour, these materials exhibit higher theoretical C_s and superior E_D compared to non-faradaic SCs. However, it has poor cycle stability due to the volume expansion during continuous charging/discharging cycles. To improve the electrochemical efficiency of TMOs, their electrical conductivity, porosity, surface area, and structural stability need to be improved. For this purpose, MOF-derived strategies are extensively employed. In this regard, Co, Fe, Zn, Ni and Mn based MOFs are widely used as sacrificial templates to prepare different types of metal oxides and their composites and they are employed as electrode materials for SCs. This section provides a thorough and critical analysis of MOF-derived metal oxides and composites, emphasising their potential as electrode materials for high E_D SC.

MOF-derived mixed metal oxide heterostructures have considered as efficient battery-type electrodes for high performance SCs because their inherited 3D architectures provide ample active sites and shortened ion transport pathways. For example, Kitchamsetti and Kim designed a hierarchical MOF-derived $CoFe_2O_4$@$NiMn_2O_4$ (CFO@NMO) composite where $CoFe_2O_4$ nanoparticles and $NiMn_2O_4$ nanoflakes interconnect into a continuous 3D network, giving more accessible active sites and faster ion/electron pathways. This structural synergy is reflected in the higher surface area of 62.2 m^2 g^{-1} and the strong electrochemical output. The prepared electrode delivers a 353.6 mAh g^{-1} specific capacity with 86.1% capacity retention after 5000 cycles. Importantly, when assembled as an aqueous hybrid SC (CFO@NMO//AC) achieves C_s of 312.8 F/g and reaches a notable E_D of 90.3 Wh/kg at a P_D of 12.9 kW/kg. The device showed nearly 100% cycling stability during the initial 2000 cycles. After 10,000 cycles, the specific capacitance gradually declined, finally maintaining 88.4% capacitance retention, while also demonstrating practical output by lighting LEDs. In-situ MOF-derived ternary metal oxides grown on NF offer a binder-free 3D scaffold with abundant active sites, improved electrolyte penetration, and fast redox kinetics [41]. In this context, P. Varatharajan and N. Vasimalai synthesized a $CoMoO_4$/$MnCo_2O_4$ (CMO/MCO) nanocomposite on NF using a Co–Mn–Mo–BDC precursor and tuning the Co:Mn ratio (1:1, 1:2 and 2:1) to optimize morphology. The 1:1 composition formed a highly porous nanoneedle architecture (FE-SEM/TEM), leading to enhanced electrochemical activity. An ASC (CMO/MCO//AC) showed strong electrochemical performance with exceptional capacitance retention after 3000 charge–discharge cycles [42]. To obtain MOF derived Fe-Mn based electrode material, Chen et al. successfully synthesized the Fe_2O_3 through calcination of Fe-MOF (MIL-88A) precursor and they make the M-Fe_2O_3@MnO_2 composite through hydrothermal technique. The optimized amount of MnO_2 coating on Fe_2O_3 reveals pinecone type core-shell composite in which MnO_2 nanosheets are vertically formed on the Fe_2O_3 and it provide excellent C_s (908.5 F/g) at lower current density in three electrode configuration. The HSC device assembled with M-Fe_2O_3@MnO_2 (anode) and $NiCo_2O_4$ (cathode) shows a wide potential window, delivering an E_D & P_D values of 86.8 Wh/kg & 804.1 W/kg, respectively. The series-connected HSCs can continuously illuminate 25 LED lights around 210 min, demonstrating their practical applicability [43].

Subsequently, a research group from china developed a Zn based mixed metal oxide nanocomposite using H_2BDC based MOF. Solvothermal reaction temperature and addition of stabilizing reagent PVP in the reaction of Zn-Co-BDC change the morphology of Zn-Co-O from hierarchical cubic structure to hierarchical coral like structure. Among them, the optimized coral-like heterostructure achieves a high C_s of 1266 F/g at low current density, maintains 91.6% stable C_s even after 10,000 cycles, and shows improved kinetics resulting from the combined effects of heterointerfaces and abundant defect sites. The assembled ASC device (Zn-Co-O//AC) achieves E_D of 78.3 Wh/kg with 90.1% capacitance retention over 10,000 cycles. During the cycling stability measurement, the specific capacitance (C_{sp}) of the assembled device slightly decreased during the initial cycles and ultimately maintained excellent cycling stability after 10,000 cycles [44] (Fig. 5(A–C)). Hameed et al. designed a comparative approach to synthesize $NiCo_2O_4$ via a calcination approach (600 °C for 3 h) using three organic linkers: H_3BTC, NDC and H_4BTEC. Among the samples, the $NiCo_2O_4$ prepared using H_3BTC (MO-1) displayed outstanding electrochemical performance, delivering a C_s of 931 F/g even at high current density, outperforming the materials derived from the other linkers. Furthermore, an asymmetric supercapacitor (ASC) fabricated using MO-1 (positive) and AC (negative) achieved a good E_D of 73.8 Wh/kg and excellent cycling stability over 10,000 charge-discharge cycles [45]. Building on such strategies, Iftikhar Hussain et al. fabricated CuO nanowire arrays on Cu mesh (CuO NWs@Cu) via a dry oxidation process. The as-prepared CuO NWs@Cu then served as conductive scaffold/template for the solvothermal growth of a Zr–Mn MOF. Zr–Mn–oxide@CuO@Cu was produced by calcining the MOF-coated electrode at a low temperature (350 °C) for 3 h. For comparison, Zr–Mn-oxide@Cu was also prepared under the same conditions but without forming CuO nanowires. SEM images confirm the unidirectional growth of CuO nanowires, which promotes uniform deposition of the Zr–Mn oxide. The final structure, which is made up of CuO nanowires adorned with polyhedral MOF-derived oxide domains, creates a hierarchical heterostructure that improves the E_D of the manufactured device by increasing the available active sites and facilitating charge transfer. The SAED pattern in TEM analysis shows the polycrystalline nature of Zr–Mn-oxide@CuO@Cu. In addition, DFT calculations suggest an enhanced/metallic-like electronic character for Zr–Mn-oxide@CuO@Cu, indicating that the Cu/CuO framework contributes to improved electrical conductivity. The assembled HSC delivered an excellent energy density of 58 Wh/kg and demonstrated good cycling stability. During the initial cycles, the C_s decreased slightly, then stabilized in the middle phase of the cycling test, and finally retained 89.5% of its original specific capacitance after 10,000 charge–discharge cycles (Fig. 4(A–F)) [46].

In a similar way, Arjit Kumar and co-workers synthesized a mixed-metal oxide (CuO–Co_3O_4) nanostructure via a bimetallic MOF-derived strategy. The resulting nanocomposite exhibits a three-dimensional (3D) interconnected morphology, consisting of nanoflakes decorated with nanoparticles, as clearly evidenced by SEM and TEM analyses. This 3D hierarchical architecture ensures improved electrode–electrolyte interaction and offers synergistic pathways for accelerated ion diffusion and continuous electron conduction. Furthermore, spin-polarized DFT calculations indicate enhanced electron-transport characteristics in the CuO–Co_3O_4 heterostructure, supporting its favourable electrochemical behaviour. The CV response in a three electrode configuration indicates the diffusion-controlled (battery-type) mechanism rather than a surface-controlled capacitive process. The redox processes occurring in the nanocomposite are described below.

$$Co_3O_4 + CuO + 2H_2O + e^- \rightleftharpoons 3CoOOH + CuOH \quad (1)$$

$$CoOOH + OH^- \rightleftharpoons CoO_2 + H_2O + e^- \quad (2)$$

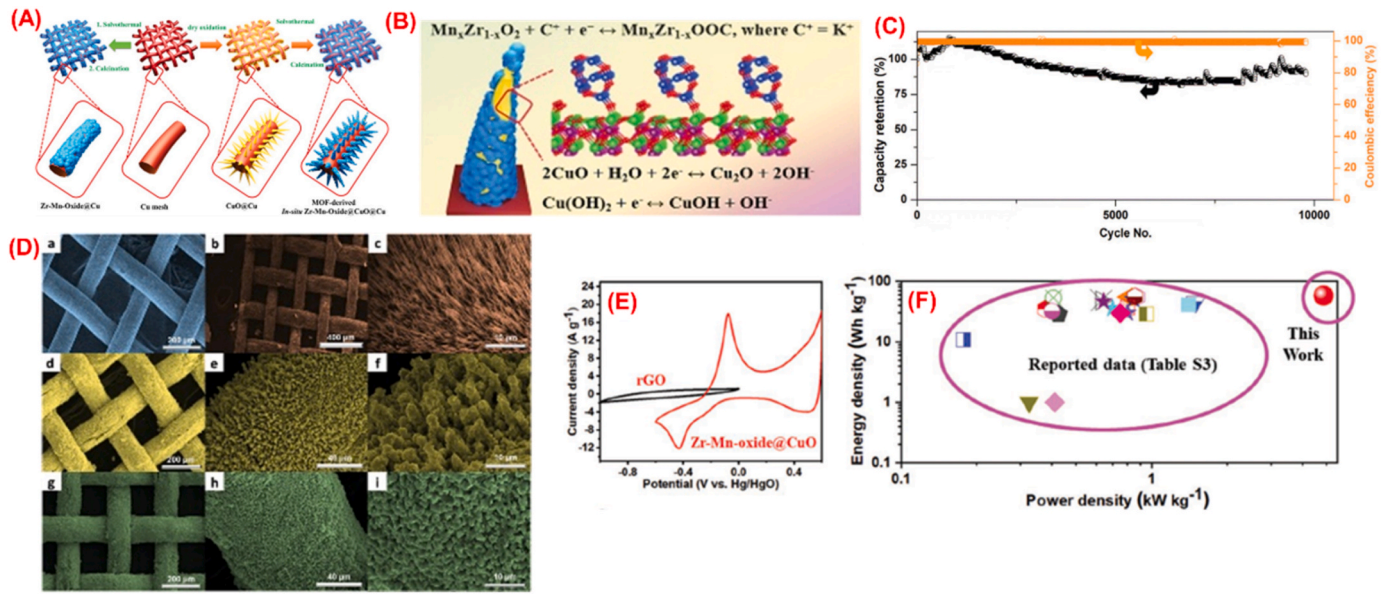

Fig. 4. (A) Conceptual diagram of the stepwise formation of bare Cu mesh, CuO NWs, Zr–Mn–O@Cu, and Zr–Mn–O@CuO@Cu architectures, (B) Illustration of the underlying electrochemical mechanism of Zr–Mn–O@CuO@Cu, (C) Cycle stability of ASC device Zr-Mn-O@CuO@Cu//rGO, (D) SEM analysis of (a) bare Cu mesh, (b–d) CuO NWs, (e–h) Zr-Mn-O@CuO@Cu, and (i) Zr-Mn-oxide@Cu, (E) Cyclic voltammetry (CV) curves of positive and negative electrode of HSC at a similar sweep rate of 10 mV /s and (F) Relation between energy density and power density values of Zr-Mn-O@CuO@Cu//rGO and reported work [46].

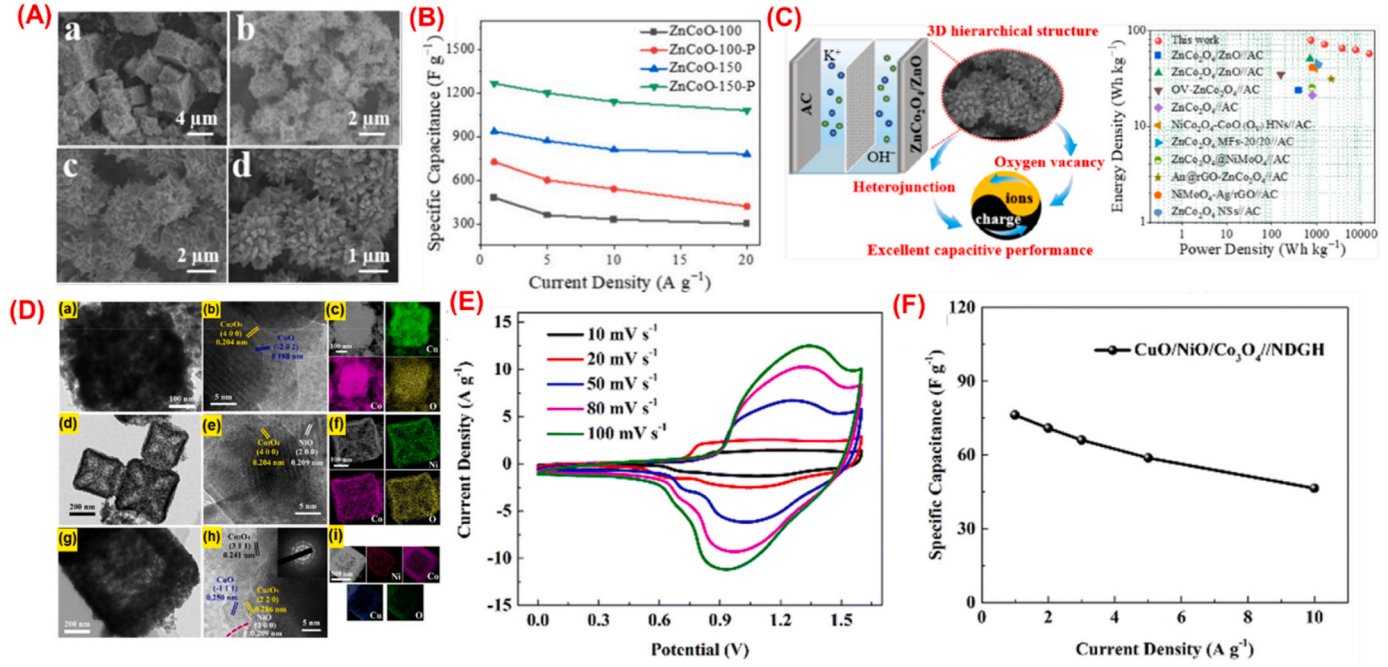

Fig. 5. (A) SEM images of ZnCoO-100 (a), ZnCoO-100-P (b), ZnCoO-150 (c), and ZnCoO-150-P (d), (B) Calculated C_s at different current densities of various electrodes, (C) Schematic representation of $ZnCo_2O_4$/ZnO//AC device and corresponding of ragone plot [44], (D) TEM and HR-TEM image of CuO/Co_3O_4 (a and b), NiO/Co_3O_4 (d and e), CuO/NiO/Co_3O_4 (g and h) and respective elemental mapping (c, f and i), (E) CV curves at various sweep and (F) C_s value of CuO/NiO/-Co_3O_4//NDGH [47].

$$CuOH + OH^- \rightleftharpoons Cu(OH)_2 + e^- \quad (3)$$

The fabricated ASC device (CuO/Co_3O_4//AC) delivers a C_s of 156 F/g at low current density. It demonstrates 91.2% capacitance retention and a 97% columbic efficiency after 10,000 GCD cycles [48].

Prussian blue analogues (PBAs) are widely employed as sacrificial templates for constructing metal-oxide heterostructures because of their open frameworks and tunable compositions enable controlled conversion into porous and hollow architectures. In this context, a research group in China reported a fabrication of NiHCC@CuHCC core-shell precursor, which was subsequently converted into a hollow trimetal oxide heterostructure (CuO/NiO/Co_3O_4) (positive) and N-doped graphene aerogel (NDGA) (negative) for an ASC. Formation of the hollow architecture was clearly evidenced by TEM, and the uniform spatial distribution of the constituent elements was verified by elemental mapping. Notably, the presence of multiple accessible oxidation states within the mixed oxides enhanced the faradaic charge-storage behaviour, leading to a strong diffusion-controlled (pseudocapacitive)

contribution relative to purely surface-controlled capacitance. As a result, the assembled ASC delivered promising energy–power characteristics along with robust cycling stability, maintaining strong performance even after 4000 charge–discharge cycles [47] (Fig. 5(D and E and F)).

2.2. MOF derived metal oxides combined carbon composite for SC application

Carbon-coated metal oxides can enhance electrical conductivity and suppress capacitance fading caused by the volume expansion of pristine metal oxides during cycling. In this regards, a solvothermal method was used to generate MOF made of FeNi-MIL-88 and NiCo-MOF-74, which served as a template material for the fabrication of mixed metal oxides ($NiFe_2O_4/NiCo_2O_4$). Furthermore, GO-integrated $NiFe_2O_4/NiCo_2O_4$ composites were prepared using a hydrothermal method. On the GO surface, the resulting $NiFe_2O_4/NiCo_2O_4$/GO displayed a mixed morphology of uniformly coated spherical and fusiform nanoparticles. Impedance analysis indicated lower charge-transfer resistance (R_{ct}) and series resistance (R_s) values, which suggest that GO significantly improved electrical conductivity in the mixed metal oxide structure. A $NiFe_2O_4/NiCo_2O_4$/GO//AC configuration was used to fabricate an ASC that produced a E_D of 109 Wh/kg with good P_D [49].

A research group from China designed a MOF–biopolymer hybrid using ZIF-67 and chitosan to produce an N-doped PC coated binary metal oxide ($CoFe_2O_4$–Fe@NC). The carbonization temperature (600–800 °C) and Fe content were tuned to optimize the structure, yielding $CoFe_2O_4$–Fe@NC-700. The carbon layer improves accessible surface area and enhances ion/electron transport, resulting in good cycling stability. A coin-cell-type ASC using $CoFe_2O_4$–Fe@NC-700 and activated carbon achieved 84.9 Wh/kg at 291.6 W/kg, confirming strong device-level performance [50]. Using similar approach, Hanamantrao and co-workers developed a fumaric-acid-based Fe-MOF as a template to synthesize C@Fe_2O_3, which was subsequently incorporated with NiO via a mechanochemical approach. The fabricated pouch-cell-type ASC device (NiO–C@Fe_2O_3//AC) retained 83.3% of its capacitance after 10,000 cycles. The device achieved an E_D & P_D values of 72 Wh/kg & 2690 W/kg, respectively at lower current density. In addition, the electrochemical properties of the fabricated SC device was tested under different bending angles [51].

Unlike conventional MOF-derived metal oxides, Kitchamsetti and Kim developed a Zn–Co MOF-derived $ZnCo_2O_4$ anchored on MXene (MX@ZCO) via an annealing strategy, where the conductive MXene scaffold suppresses restacking/agglomeration and promotes continuous electron transport. The $ZnCo_2O_4$ coating further introduces abundant redox-active sites and creates more accessible ion-diffusion channels. BET adsorption–desorption isotherms indicate a mesoporous texture, and the composite shows a high specific surface area (40.21 $m^2\ g^{-1}$) compared with pristine MXene (23.9 m^2g^{-1}) and $ZnCo_2O_4$ (25.2 m^2g^{-1}), consistent with its improved charge-storage behaviour. Electrochemically, the MX@ZCO electrode delivers a high specific capacity (reported as 260 mAh g^{-1} at a low current density), though both capacitance retention and columbic efficiency gradually decline upon prolonged cycling. When assembled into an ASC (MX@ZCO//AC), the device operates over a widened voltage window of 1.6 V (from CV &GCD), achieving a exceptional E_D and P_D of 63.89 Wh/kg and 10.337 kW/kg respectively, which highlighting the benefit of MXene–MOF-derived oxide synergy for the fabrication of HSCs [52].

Mateen et al. reported a MOF mediated fabrication approach to build a binder-free cobalt-oxide nanosheet cathode on carbon fibre cloth (Co-O-NSs@CFC). FESEM reveals a distinctive walnut-like “nano-reservoir” nanosheet array uniformly covering the cloth, creating abundant cavities and interconnected mesopores. N_2 adsorption–desorption isotherms further verify the mesoporous architecture, delivering a specific surface area of 56 m^2 /g with good porous nature. This supports fast ion movement and improved electrolyte accessibility. The prepared electrode delivers high pseudocapacitance and, when assembled into a flexible ASC (Co-O-NSs@CFC||AC) with PVA/KOH gel, the device achieves C_S of 178 F/g, E_D of 55.7 Wh/kg at low current density and exceptional capacitance retention after 5000 numbers of GCD cycles, demonstrating strong promise for wearable energy storage [53]. Xin Sun et al. fabricated an anode material for an ASC using a MOF-derived strategy. First, a Bi-MOF was synthesized by hydrothermal method using H_3BTC, followed by conversion to a BM/BiOCOOH intermediate through a solvothermal process. The resulting precursor was then transformed into a porous Bi_2O_3/C composite by controlled pyrolysis. For the cathode, B-rGO/NiCoB was prepared via a chemical reduction route. The MOF-derived carbon skeleton effectively buffers the volume expansion of Bi_2O_3 and enhances structural integrity, thereby improving electrochemical stability. Notably, the assembled B-rGO/Ni-CoB//Bi_2O_3/C device delivers an E_D of 50.4 Wh/kg, highlighting the synergistic integration of MOF-derived porous anodes with defect-rich amorphous boride cathodes to achieve both high E_D and durable cycling performance [54].

Yin et al. reported a ZIF-67 MOF-derived strategy to construct self-supporting $NiCo_2O_4$ nanocages grown on SiC-nanowire-coated carbon cloth (CC/SiCNWs), yielding a flexible and binder-free electrode (CC/SiCNWs@$NiCo_2O_4$ NCs) for HSCs. SEM and TEM analysis revealed a “sugar-gourd-like” hierarchical porous architecture uniformly anchored on the conductive cloth. This interconnected, porous framework is advantageous because it exposes abundant redox-active sites, shortens ion-diffusion pathways, and provides an efficient electron-transport network. Electrochemical measurements in a three-electrode configuration (CV and GCD) indicated predominantly Faradaic (battery-type) charge storage. Kinetic analysis using Dunn's method further suggested that the charge storage is mainly diffusion-controlled, with a smaller capacitive contribution. In three electrode configuration, the electrode delivered a C_s of 1377.6 F/g at low current density. The assembled HSCs showed excellent electrochemical performance, achieving an E_D of 46.58 Wh/kg and retaining 89.9% capacitance after 3000 cycles [55] (Fig. 6(A–C)). A research group from China reported the fabrication of a ZIF-67/Co array on an Au electrode using a solvent-free chemical deposition strategy. The as-prepared ZIF-67/Co array was subsequently transformed into a CoO_x/carbon composite array through calcination and then used as the positive electrode for assembling an ASC. Morphological analysis revealed that the polyhedral ZIF-67 crystals were uniformly grown on a tree-like cobalt array, which evolved into a flake-like architecture after calcination, as confirmed by cross-sectional SEM observations. The resulting CoO_x/carbon composite arrays exhibited reduced ion-diffusion pathways, pronounced pseudocapacitive behaviour originating from the TMOs, and improved conductivity contributed by the carbon framework. The assembled ASC displayed hybrid capacitive characteristics which delivered a high C_s and the device demonstrated good cycling stability. It maintained stable performance during the initial 4000 cycles. Thereafter, the cycling stability slightly declined, but it still retained a good specific capacitance retention after 10,000 cycles [56].

Similarly, Acharya et al. prepared porous carbon nanofibers (PCNFs) via an electrospinning technique. They employed an MOF-derived strategy to construct vertically aligned bimetallic Ni–Fe oxide/nanoporous carbon (Ni–Fe–O/NPC) nanoarchitectures on a PCNF. HR-TEM images clearly revealed the growth of tetrahedral nanorods on the PCNF. The fabricated electrode offers more electroactive sites and shorter electron-transport routes because of its large surface area and enhanced porosity. The electrode material calcined at 400 °C delivered the highest C_s (1419 F/g) in a three-electrode setup compared with samples calcined at other temperatures. Additionally, an ASC device was put up utilising KOH as the electrolyte and Ni–Fe–O/NPC/PCNF (positive) and Fe_2O_3/NPC/PCNF (negative). The fabricated device exhibited a maximum C_s of 116.13 F/g and maintained 81.3% capacitance retention. EIS analysis both before and after cycling demonstrate ASC's steady electrochemical properties [57] (Fig. S1 (A-D)). S. Silambarasan

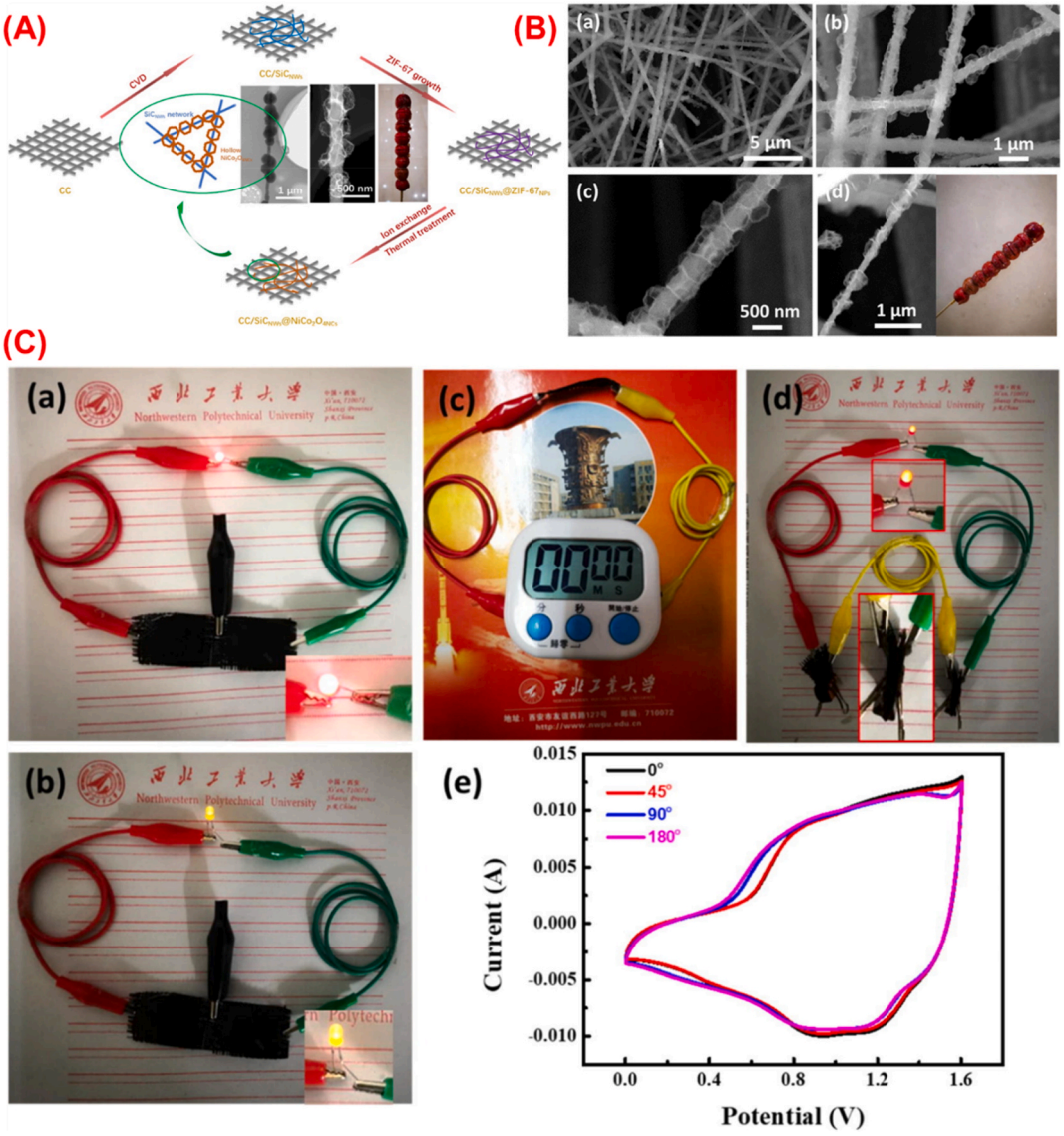

Fig. 6. (A) Diagrammatic illustration of the preparation of CC/SiCNWs@$NiCo_2O_4$NCs, (B) SEM images of CC/SiCNWs@$NiCo_2O_4$NCs (a-d), (C) Photographs showing (a) red and (b) yellow LEDs powered by two devices connected in series, (c) an electronic display driven by a single device, and (d) red LEDs operated by two devices under bending conditions; (e) CV curves of the device at various bending angles [55].

et al. synthesized a bimetallic MOF-derived Ni-doped Co_3O_4@N-doped carbon nanospheres (Ni_x–Co_3O_4@NCS) through a simple calcination route. The Ni doping level in Co_3O_4@NCS was systematically tuned to optimize the electrochemical performance. Among the different compositions, Ni_x–Co_3O_4@NCS-2 exhibited the highest C_s and good rate capability in three-electrode configuration. Furthermore, the fabericated ASC device (Ni_x–Co_3O_4@NCS-2//AC) delivered an E_D of 26.3 Wh/kg at 416.7 W/kg of P_D at a low current density, demonstrating its promise for practical high-performance energy storage [58]. In a similar approach, Han et al. prepared a MOF-derived 3D hollow nitrogen-doped carbon/Fe_2O_3 core–shell composite (NHCs@ Fe_2O_3) as a negative electrode material for high-performance SCs. The prepared electrode exhibited a high specific surface area of 219.36 m^2 /g, mesoporous channels of approximately 8.8 nm, shortened ion-diffusion pathways, and improved electrical conductivity. The authors further fabricated an asymmetric pouch-type SC using NHCs@Fe_2O_3 as the negative electrode and $CuCo_2S_4$@NiFe-LDH as the positive electrode. The assembled device delivered specific capacitance values of 193 F/g at current density of 1 A/g. Moreover, the device achieved a high energy density of 68.6 Wh/kg at a power density of 828.9 W/kg. The cycling stability profile of the ASC device showed an unusual trend, where the capacitance retention sharply decreased during the initial cycles then gradually stabilized and maintaining 81.9% capacitance retention after 10,000 cycles. These results confirm the strong practical applicability of the NHCs@Fe_2O_3//$CuCo_2S_4$@NiFe-LDH pouch-type ASC for high-energy-density energy storage devices [59]. The comparative performance of metal oxides and metal oxide/carbon composites is summarized in Table 1 and Table S1.

Several other research groups have also published research articles in the field discussed above. Kuen-Chan Lee and his group prepared MOF-derived spinel $NiMn_2O_4$/$CoMn_2O_4$ and applied it for both SC and photocatalysis applications. The fabricated ASC device achieves excellent E_D and P_D values [66]. Another research group from India fabricated $NiCo_2O_4$ nanosheets through a sacrificial MOF-templated approach. The fabricated electrode exhibits superior electrochemical performance in both two-electrode and three-electrode configurations [67]. Similarly, Rakhee Bhosale et al. prepared a bimetallic MOF ($MnFe_2$-MOF) using a solvothermal approach, which was subsequently converted into $MnFe_2O_4$ nanostructures through calcination. The prepared electrode exhibited good cycling stability (85.25%) with columbic efficiency of

Table 1
Comparative analysis of MOF derived binary and ternary metal oxides and their composites: synthesis methods and electrochemical parameters.

S. No	Type of MOF	MOF derived material	Synthesis method	Capacitance (Three Electrode)	Type of two electrode system	E_D Wh/kg & P_D W/kg	Cycle stability	Ref
1.	FeCo-MIL-88 MOF	$CoFe_2O_4$ @$NiMn_2O_4$	solvothermal and Calcination	353.6 mAh/g @ 4 mA/g	ASC- $CoFe_2O_4$ @$NiMn_2O_4$//AC	90.3 & 1367	88.4 % - 10,000 cycles	[41]
2.	Co–Mn–Mo-BDC	$CoMoO_4$/$MnCo_2O_4$/NF	Solvothermal and calcination	1782 F/g @ 1 A/g	ASC- $CoMoO_4$/$MnCo_2O_4$/NF//AC	90 & 2800	90 % −3000 cycles	[42]
3.	Fe-MOF	Fe_2O_3@MnO_2	MOF sacrificial template + hydrothermal	908.5 F/g @ 1 A/g	ASC-Fe_2O_3@MnO_2// $NiCo_2O_4$	86.8 & 804.1	78.7% - 8000 cycles	[43]
4.	ZnCo-MOF	$ZnCo_2O_4$/ZnO	Solvothermal and thermal oxidation	1266 F/g @ 1 A/g	ASC- $ZnCo_2O_4$/ZnO//AC	78.3 & 750	90.1 % - 10,000 cycles	[44]
5.	Ni–Co bimetal MOF	$NiCo_2O_4$	mechanochemical grinding and calcination	913.5 F/g @ 7 A/g	ASC- $NiCo_2O_4$//AC	73.83 & 1181.2	95.7 % −10 000 cycles	[45]
6.	Zr-Mn-MOF	Zr-Mn-oxide@CuO@Cu	solvothermal and Calcination	458.33 F/g @ 4 A/g	ASC- Zr-Mn-oxide@CuO@Cu//rGO	58 & 4855	89.5% - 10000 cycles	[46]
7.	Bimetallic Cu–Co MOF	CuO–Co_3O_4	Co-precipitation and anneling	1564.4 F/g @ 1 A/g	ASC- CuO–Co_3O_4//AC	48.7 & 750	91.2 % - 10,000 cycles	[48]
8.	Ni-CO-PBA	CuO/NiO/Co_3O_4	Co-precipitation and calcination	262.5 F/g @ 1 A/g	ASC- CuO/NiO/Co_3O_4//N-graphene hydrogel	27.1 & 1037.5	100.7% −4000 cycles	[47]
MOF derived Metal Oxide with Carbon Composites								
9.	FeNi-MIL-88/ NiCo-MOF-74	$NiFe_2O_4$/$NiCo_2O_4$/GO	Hydrothermal synthesis calcination	1470 F/g @ 1 A/g	ASC- $NiFe_2O_4$/$NiCo_2O_4$/GO//AC	109 & 1051	90.7% - 1000 cycles	[49]
10.	ZIF-67	$CoFe_2O_4$-Fe@NC	Co-presipiatation and carbonization	3960.9 F/g @ 1 A/g	ASC: $CoFe_2O_4$-Fe@NC-700//AC (coin-cell)	84.9 & 291.6	94.9%- 10,000 cycles	[50]
11.	Fe-MOF (MIL-88A)	NiO–C@Fe_3O_4	Hydrothermal and calcination	1210 F/g @ 1 A/g	ASC-NiO–C@Fe_3O_4//AC	72 & 2690	83.32%- 10,000 cycles	[51]
12.	ZIF-67	NHCs@Fe_2O_3	Co-precipitation and calcination	264 F/g @ 3 A/g	ASC-NHCs@Fe_2O_3// CuCo2S4@NiFe-LDH	68.6 & 828.9	81.9% - 10,000 cycles	[59]
13.	ZnCo-MOF	MXene @ZnCo2O4	Hydrothermal and Calcination	260 mAh/g @ 1 mA/g	ASC- MXene @$ZnCo_2O_4$// AC	63.8 & 3512.2	91.3%- 15,000 cycles	[52]
14.	ZIF-67 (Co-MOF)	Co-O-NSs @ CFC	Hydrothermal & calcination	842 F/g @ 1 A/g	ASC- Co-O-NSs @ CFC//AC	55.7 & 1125.9	94.5% - 5000 cycles	[53]
15.	Bi-MOF	Bi_2O_3/C	Calcination and chemical reduction	1029 F/g @ 1 A/g A/g; 1204.4 F/g @ 1 A/g	ASC- Bi_2O_3/C//B-rGO/ NiCoB	50.4 & 800	96.21 % −10 000 cycles	[54]
16.	ZIF-67	CC/SiCNWs@$NiCo_2O_4$ hollow nanocages	CVD growth, ion exchange and anneling	1377.6 F/g @ 1 A/g	ASC- CC/ SiCNWs@$NiCo_2O_4$//AC	46.58 & 800	89.9% −3000 cycles	[55]
17.	ZIF-67 (Co-MOF)	CoOx/carbon composite array	Electrodeposition, carbonization and oxidation	1660.4 F/g @ 1 A/g	ASC- CoOx/carbon composite array//AC	40 & 400	100% - 10,000 cycles	[56]
18.	Ni-Fe-MOF	Ni–Fe–O/NPC/PCNFs	Hydrothermal and Calcination	1419 F/g @ 1 A/g	ASC- Ni–Fe–O/NPC/ PCNFs//Fe2O3/ NPC@PCNFs	41.3 & 892.2	78.6% - 20,000 cycles	[57]
19.	Co-MOF	Ni-doped Co_3O_4/NCS carbon nanospehere	Hydrothermal and Calcination	1284 F/g @ 1 A/g	ASC- Ni-doped Co3O4/ NCS//MWCNT	26.38 & 416.7	92% - 3000 cycles	[58]
MOF derived metal hydroxide and their composites								
20.	ZnCo-MOF	ZnNiCo-LDH/CuO-Cu foam	Calcination and Hydrothermal	378.10 mA h/g @ 1 A/g	ASC- ZnNiCo-LDH/CuO-Cu foam//CNT	117.5 & 576.9	92.3%- 10,000 cycles	[60]
21.	Bimetallic ZnCo-ZIF	ZnCoNi LDH@Mxene	Solvent mediated, ion-exchange	1414 F/g @ 1 A/g	ASC- ZnCoNi LDH@Mxene//AC	45.6 & 750	63 % −8000 cycles	[61]
22.	ZIF-67	NiCo-LDH@C	Co-precipitation and etching process	2210.6 F/g @ 1 A/g	ASC-NiCo-LDH@C//RGO	45.02 & 799.96.	86.3% −10,000 cycles	[62]
23.	Fe-MOF	Ni-Fe-OH@PCNFs	Electrospinning and hydrothermal	1528 F/g @ 1 A/g	ASC- Ni-Fe-OH@PCNFs// Fe_2O_3/NPC@PCNFs	44.3 & 907	83.2 % - 10,000 cycles	[63]
24.	Co-MOF-74	$La(OH)_3$@$Cu(OH)_2$/$Co(OH)_2$/NF	Solvothermal, ion-exchange and electrodeposition	874.8 F/g @ 1 A/g	ASC- $La(OH)_3$@$Cu(OH)_2$/ $Co(OH)_2$/NF//AC	43.9 & 775	76.4 % - 11,000 cycles	[64]
25.	NiCo-MOF	NiCo-LDH@$Ni(OH)_2$	Solvothermal and alkalization	1509.6 F/g @ 1 A/g	ASC- NiCo-LDH@Ni(OH)// AC	30.6 & 799.9	89% - 5000 Cycles	[65]

*ASC-Asymmetric Supercapacitor, E_D-Energy Density and P_D-Power Density.

96.81% in ASC device configuration [68]. Jiaying Zhang et al. fabricated $NiO/V_2O_3/C$ heterojunction nanostructures using a MOF-derived approach. The prepared ASC ($NiO/V_2O_3/C//AC$) delivered an excellent E_D of 26.6 Wh/kg and P_D of 400 W/kg, along with outstanding cycling stability [69].

2.3. MOF derived metal hydroxide and their composite for SC application

MOF-derived multimetal hydroxides, particularly their composites with conductive metal oxides and carbon-based materials, have emerged as potential electrode materials for energy storage applications because of their reversible redox processes, favourable oxidation states, and good structural integrity [70]. In this context, M. Poudel et al. fabricated a ZnNiCo-LDH grown on vapor-solid-phase–derived CuO nanowire arrays directly anchored on Cu foam and this in-situ grown method forms ZnNiCo-LDH/CuO-Cu binder free nanohybrids for SC application. The vertically align CuO nanowire on Cu foam act as a conductive backbone and MOF derived ternary metal LDH produce enlarged electrochemically accessible surface area and ample redox-active sites. The fabricated ASC with ZnNiCo-LDH/CuO-Cu (positive) and nitrogen doped CNT (negative) exhibits specific capacity of 148.9 mAh g^{-1}. The cycling stability test showed a gradual decrease in capacitance retention, maintaining 92.1% of its initial C_s after 10,000 charge–discharge cycles [60]. Using similar approach, Min Lu et al. reported the fabrication of hierarchical ZnCoNi-LDH@MXene composite by ZnCo-MOF precursor through solvent mediated template-etching approach forming an interconnected mesoporous and continuous electron transport network. Due to the presence of multiple redox centers, optimized pore architecture, and strong interfacial coupling, the composite material delivers a good C_s of 1414 F/g and retained 77.8% capacity at 10 A/g. The fabricated ASC exhibits an E_D of 45.6 Wh/kg at 750 W/kg with good cycling durability [61].

To improve the internal conductivity and cyclic stability of LDH based electrodes, Junzhuo Yuan and his group members developed MOF derived carbon combined LDH architecture act as a. In that reported work, flower-like hierarchical NiCo-LDH@C nanostructure on CC was rationally designed using carbonized ZIF-67 which act as a both conductive scaffold and a nucleation template. The MOF derived Co@C framework provides uniformly deposited Co nanoparticles act as an anchoring centers which facilitate the tight grown of NiCo-LDH ultrathin nanosheets. The synergistic effect of NiCo-LDH and carbon skeleton provides high C_s of 2210.6 F/g at lower current density with excellent rate capability (88.8% at 10 Ag^{-1}). Finally, the ASC assembled with NiCo-LDH@C//RGO delivers a high E_D of 45.02 Wh/kg at a P_D of 799.96 W/kg [62]. In a similar way, Acharya et al. developed a transmogrification strategy to in-situ deposition of Fe-MOF on electrospun porous carbon nanofibers (PCNFs) were chemically transformed into interconnected Ni-Fe-LDH anchored on PCNF. Unlike conventional co-precipitation approach for the preparation of LDH, MOF derived approach provides controlled metal-ion leaching and re-precipitation. MOF derived Ni-Fe-LDH shows pellet like morphology which provides accessible surface area and fast ion transport. The optimized Ni-Fe-LDH/PCNF binder free electrode exhibited a surface area of 74.3 m^2g^{-1} with mesoporous nature and the prepared electrode delivers faradaic based charge storage kinetics thorough involving reversible Ni^{2+}/Ni^{3+} and Fe^{2+}/Fe^{3+} redox couples. Compared to single hydroxide and bimetal hydroxides synthesized without the MOF template, Ni-Fe-LDH/PCNF shows higher C_s of 1528 F/g at 1 A/g and maintained 87.6% of capacitance retention over 10,000 cycles. An ASC assembled using Fe_2O_3/N-doped PCNF as the negative electrode and Ni-Fe-LDH/PCNF as the positive electrode exhibits a broad operating voltage window of 1.0–1.5 V, achieving an E_D of 44.3 Wh/kg at a P_D of

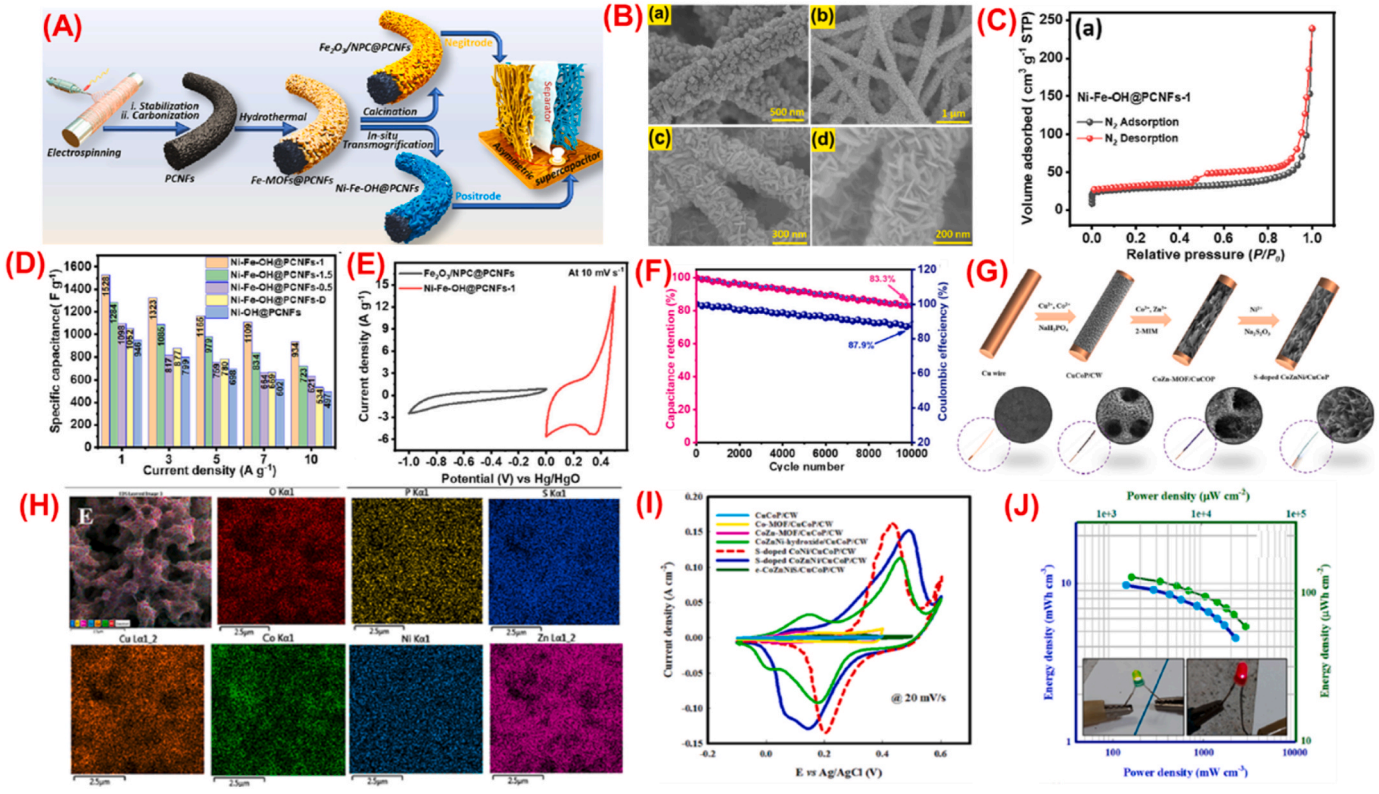

Fig. 7. (A) Diagrammatic representation of the synthesis route for ASC electrode materials, (B) FE-SEM observations of (a) Fe-MOFs@PCNFs and (b–d) Ni–Fe–OH@PCNFs-1; (C) N_2 adsorption–desorption isotherm curve of Ni–Fe–OH@PCNFs-1, (D) Bar diagram of C_s vs current densities of different electrode, (E) CV profiles of Fe_2O_3/NPC@PCNFs and Ni–Fe–OH@PCNFs-1 at a scan rate of 10 mV/s; (F) cycling stability and Coulombic efficiency of the ASC device during 10,000 GCD cycles [63], (G) Diagrammatic representation of MOF-derived S-doped CoZnNi–OH/CuCoP/CW; (H) EDS mapping of CoZnNi–OH/CuCoP/CW; (I) CV curves of various microelectrodes at 20 mV/s; (J) Ragone plot of the fabricated fiber micro-SC [71].

907 W/kg. This work clearly demonstrate that MOF to LDH modified transmogrification on conductive fibrous scaffolds act as an excellent binder free electrode for SC application (Fig. 7(A–F)) [63].

Another research group from China employed a similar etching-based strategy to prepare a MOF-derived core–shell-type ternary hydroxide $La(OH)_3$@Cu/Co-LDH on a binder-free NF electrode which exhibits exceptional electrochemical performance. This approach effectively overcomes the intrinsic limitations associated with single-metal LDHs deposited on substrates using conventional deposition techniques. In the synthesis process, MOF-74 microrods were first grown on NF and subsequently converted into Cu/Co-LDH via an ion-exchange method. Thereafter, $La(OH)_3$ was uniformly coated onto the Cu/Co-LDH through an electrodeposition technique. The resulting electrode delivered a high C_s of 875 F/g at 1 A/g, along with excellent rate capability in a three-electrode configuration. Furthermore, the assembled ASC ($La(OH)_3$@Cu/Co-LDH//AC) achieved a high E_D of 44 Wh/kg and demonstrated outstanding cycling stability, retaining performance over 11,000 charge–discharge cycles [64]. Another research group from china developed a terephthalic acid based Ni-Co-MOF derived nanosheet assembled heterogeneous NiCo-LDH/$Ni(OH)_2$ composite through solvothermal reaction followed by stirring under alkalization condition which preserving the structural integrity of the prepared composite. By changing the Ni/Co ratio (2:1), NiCo-LDH/$Ni(OH)_2$ prepared with 2D porous nanosheet architecture, enhanced electro active surface area and improved ion-transport pathways. This prepared electrode material delivers diffusion based redox behaviour with high specific capacity of 754.8C/g at 1 A/g [65].

A research group from Taiwan reported a simple and cost-effective strategy to fabricate a binder-free MnCo-LDH nanosheet array on NF. First, the Co-MOF prepared via a co-precipitation approach was deposited on NF, and subsequently, MnCo-LDH was formed on the NF through an etching process. Structural and spectroscopic analysis confirmed the formation of hydrotalcite-like MnCo-LDH. The XPS analysis confirmed the metal-oxygen environment and hydroxyl rich surfaces favourable for faradaic reaction. The assembled ASC MnCo-LDH//AC maintained 78% of its initial capacitance after 5000 charge/discharge cycles [72].

MOF derived hierarchal nanoarchitectures on 1D current collectors are highly effective in overcoming the intrinsic limitations of fiber based energy storage devices. In this context, Leila Naderi and Saeed Shahrokhian reported a 2D-3D mixed nanoarchitecture on copper wire (CW) in that 2D S-doped CoZnNi-OH nanosheet arrays derived from Co-Ni-MOF and vertically integrated onto 3D dendritic CuCoP nanoarrays grown on a CW substrate. The prepared MOF derived nanosheet structure with CuCoP nanoarrarys on CW provides high mesoporous nature, multivalent metal redox centers and surface defects which improve the redox based charge storage and electro active surface area of electrode. As result, the S-doped CoZnNi-OH/CuCoP/CW microelectrode provide high areal/volumetric/length capacitance of 2.9 F /cm^2, 290 F /cm^3 and 348 mF /cm at lower current density, respectively. The electrochemical kinetic analysis confirm the microelectrode prepared through MOF derived approach delivers higher OH^- diffusion coefficients that much greater than the microelectrode prepared through electrodeposition approach. Furthermore, the fabricated solid state wire type micro supercapacitor assembled with V_2O_5-PPy/rGO-nanocellulose hydrogel negative microelectrode achieved excellent areal E_D of 127.62 μWh/cm^2 at a P_D of 1.83 mW/cm^2 and it is also maintains exceptional mechanical stability and durability (Fig. 7(G–J)) [71]. The comparative performance of metal hydroxide and their composites is summarized in Table 1 and Table S1 while the performance of flexible SC devices is provided in Table S2.

2.4. MOF derived metal sulfides and their composite for SC application

Different types of metal oxides and their composites have been extensively studied as cathode materials for SCs. In this context, MOF-derived metal sulfides are widely used as electrode materials for SC applications due to their higher electrical conductivity and faster redox kinetics, which contribute to improved electrochemical performance. Importantly, the metal-sulfer bond is less ionic then the metal-oxygen bond which can improve the charge transfer and enhanced electrochemical activity. However, they still face challenges related to cycling stability and rate capability. These limitations can be alleviated by rational control over structure and morphology, in situ fabrication of self-supported electrodes, and the development of hierarchical nanostructured composites integrated with carbon-based materials [73–75].

Y. Abbasi et al. fabricated MOF derived Ni/Cu sulfides combined MWCNT as electrode material for electrochemical application. In that work, Cu-MOF (HKUST-1) acts both as a Cu source and structural template of the formation of bi-metal sulfides followed by incorporation of MWCNT by ultrasonication method to improve electrical conductivity and electro active surface area. The prepared electrode material exhibits good electrochemical performance in symmetrical device configuration and it also used as an electrocatalyst for methanol oxidation. The fabricated SSC device consists of wider potential window and high E_D [76]. H. Guo et al. fabricated the Ni-Cu-sulfides combined porous-MXene (p-MXene) nanocomposite with sandwich like heterostructure. First Ni-MOF prepared by H_2BDC organic linker was grown in-situ way on the conductive p-MXene substrate through solvothermal approach and Cu was incorporated with the sulfurization reaction which subsequent convert Ni-MOF into Ni_3S_4 with form CuS on the surface of p-MXene. The prepared heterostructure delivers high C_s 1917 F/g at 1 A/g compared to p-MXene@Ni-MOF (866 F/g at 1 A/g) along with good rate capability and low charge transfer resistance. The electrode also showed excellent cycling durability, retaining 91% capacitance after 30,000 cycles in three electrode configuration, highlighting the structural stability provided by the MXene-supported sandwich architecture (Fig. S2 (A to C)) [77].

Similarly, one of the research group from china developed a core shell type MOF derived nitrogen-doped porous multishell CuCoS@Ni-CoS nanospheres (N–CCS@NCS) to synergistically enhance the performance in SC and hydrogen evolution reaction (HER). First they make Cu-Co-O double core shell structure and it was coated with Ni-Co-MOF nanoclusters. Further, the framework structure covert as metal sulfide through sulfurization reaction which gives multi-shell N–CCS@NCS nanosphere. Importantly, the shell numbers, thickness and shell density can be adjust by the change Ni concentration. The well-engineered multishell architecture of N–CCS@NCS provides greater access to reactive sites and promotes rapid ion/electron transport, thereby improving charge-storage kinetics. The prepared electrode material provides a high surface area and a well-developed mesoporous network, which enhances electrolyte penetration and lowers charge-transfer resistance, resulting in strong pseudocapacitive behaviour in an alkaline electrolyte. When assembled into an asymmetric device (N–CCS@NCS//AC), it delivers an E_D of 87.3 Wh/kg at 825 W/kg and retains 81.3% of its capacitance after 8400 cycles, demonstrating good device-level durability [78].

Another research group from china fabricated the Al-MOF derived metal sulfides directly coated on NF with amorphous/crystalline phase (a/c-Co(Al)S-1) where Al, N and C eventually coordinate with amorphous phase. The a/c-Co(Al)S-1 exhibits 3D network with very loosely stacked ultrathin nanosheets and it provides high surface area, more accessible redox active sites then a/c-Co(Al)S-2 prepared through CoAl-MOF template method. The a/c-Co(Al)S-1 electrode delivered a high specific charge of 1791.8C/g at 1 A/g, superior rate capability, and excellent cycling stability then their oxide intermediated (CoAlO) and a/c-Co(Al)S-2. The electrochemical kinetic study reveals that diffusion controlled battery-type mechanism which confirms the efficient ion accessibility within the hierarchical porous framework. The fabricated HSC (a/c-Co(Al)S-1//AC) operated stably up to 1.6 V and achieved a high E_D of 77.1 Wh/kg at 800 W/kg P_D, capacitance retention gradually decreased and finally maintained 87.4% over 10,000 cycles (Fig. 8(F–I)) [80]. Liu et al. fabricated the Zn-Co-MOF derived ZnS/Co_3S_4/$Ti_3C_2T_x$

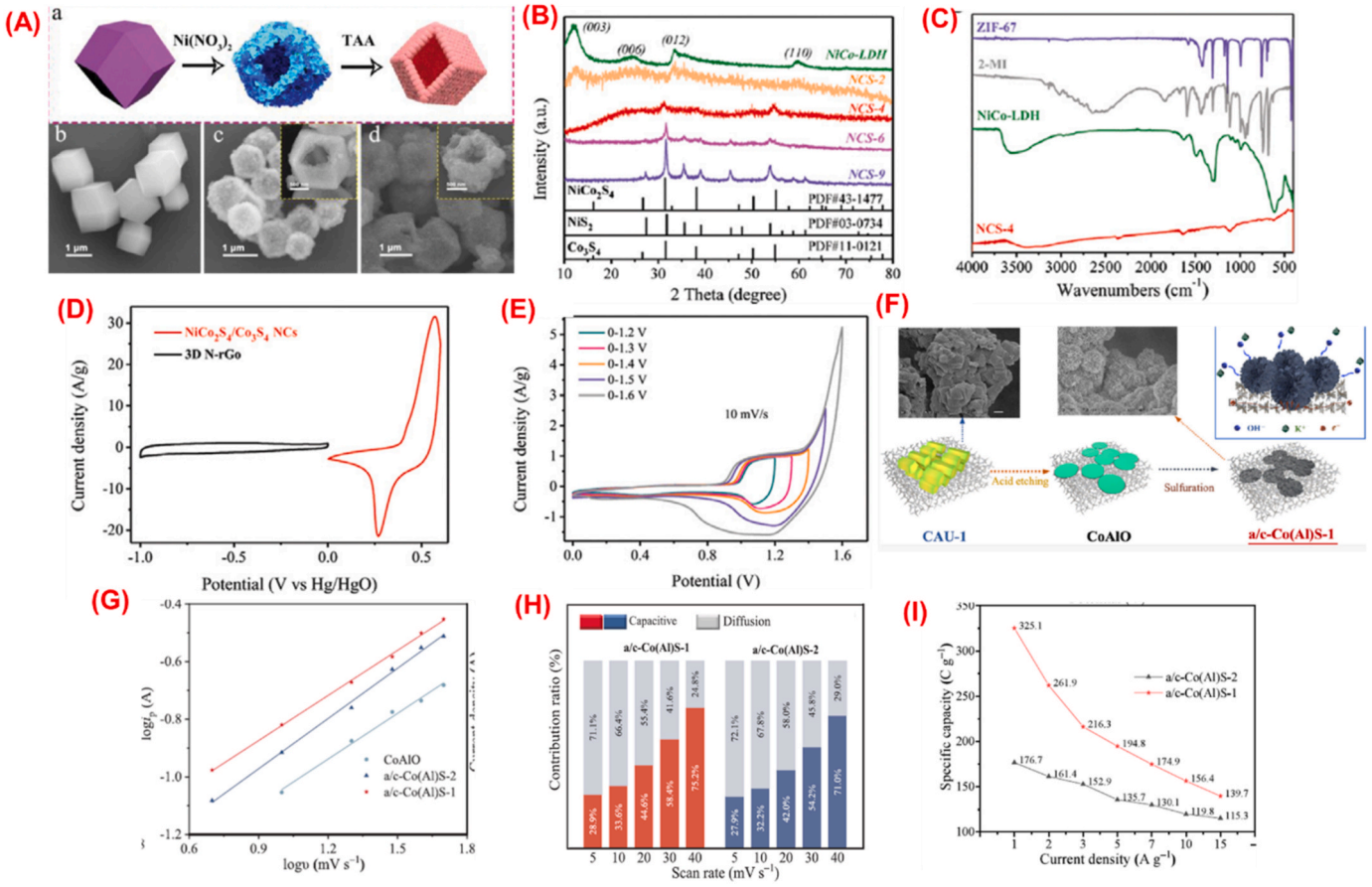

Fig. 8. (A) (a) Diagrammatic representation of the synthetic direction of $NiCo_2S_4/Co_3S_4$ NCs. (b) FESEM characterization of ZIF-67 crystals; (c) FESEM and (f) TEM images of NiCo–LDH; (d) FESEM images of $NiCo_2S_4/Co_3S_4$ NCs; (B) X-ray diffraction patterns of NiCo–LDH, NCS-2, NCS-4, NCS-6, and NCS-9, (C) FTIR analysis of ZIF-67, 2-MI, NiCo–LDH, and NCS-4; (D) CV responses of $NiCo_2S_4/Co_3S_4$ and N-rGO electrodes measured at 5 mV/s, (E) CV curves recorded at different voltage ranges at 10 mV/s [79], (F) Diagrammatic representation for the synthesis procedure of a/c-Co(Al)S-1, (G) Plots of log i_{pa} vs log υ for the CoAlO, a/c-Co(Al)S-2 and a/c-Co(Al)S-1, (H) capacitance contributions for the a/c-Co(Al)S-1 (red area) and a/c-Co(Al)S-2 (blue-gray area) at different sweeping rates and (I) C_s of assembled ASC deivce at different current densities [80].

MXene directly grown on NF through in-situ solvothermal and sulfurization strategy. The prepared heterostructure on NF exhibits hierarchical architecture, high pesudocapacitance characteristics from bi-metal sulfides and excellent electrical conductivity, mechanical stability from MXene structure. The optimized $ZnS/Co_3S_4/Ti_3C_2T_x$ MXene delivers excellent C_s of 2193.8 F/g at 1 A/g. DFT calculation further theoretically studies the charge distribution and electron transport of prepared material. The constructed ASC device with $ZnS/Co_3S_4/Ti_3C_2T_x$ MXene (positive) and AC (negative) electrodes which delivers a high E_D of 66.9 Wh/kg at a P_D of 750 W/kg, demonstrating the effectiveness of MOF-derived sulfide/MXene heterostructures for energy storage application [81]. CNTs interpenetrating with MOF derived Co-Ni-S to form a 3D interconnected morphological nature was fabricated by Zhenlin Ma et al. The 3D interconnected morphology of CNT/Co-Ni-S nano-hybrids provides fast electron transfer and pesudocapacitive behaviour. Dunn's method was used to estimate the percentage of capacitive contribution of the CNT/Co–Ni–S-based electrode at different scan rates. The analysis indicates that the prepared electrode exhibits a higher diffusion-controlled contribution rather than purely surface capacitive behaviour. The estimated C_s of the CNT/Co–Ni–S electrode (540.6C/g at 1 A/g) is 2.5 and 5 times higher than that of Co_3S_4/CNTs and pristine Co_3S_4, respectively. Furthermore, the fabricated ASC device (CNT/Co–Ni–S//AC) exhibited good electrochemical performance over a wide potential window. During cycling, the capacitance retention gradually decreased in the initial 4000 cycles and ultimately retained 83% of its initial capacitance after 10,000 charge–discharge cycles (Fig. S2 (D – F)) [82].

P. Naveenkumar et al. developed a MOF derived sulfide heterostructure ($CuCo_2S_4$@FeS_2) for ASC application. First the $CuCo_2$-MOF was prepared by trimesic acid in DMF through solvothermal approach then $CuCo_2S_4$ with carbon phase derived from $CuCo_2$-MOF through annealing process in the presence of sulfer and FeS_2 nanoplates directly grown on $CuCo_2S_4$ through hydrothermal reaction. The BET analysis confirms the prepared hybrids exhibits mesoporosity and importantly contains a larger mean pore diameter (~72 Å), which supports electrolyte penetration and rapid ion transport. The fabricated ASC ($CuCo_2S_4$@FeS_2//AC) exhibits C_s of 204.77C/g at 1 A/g. The estimated E_D values is 63.99 Wh/kg at 1125 W/kg (P_D) and it maintains 90% capacitance retention after 10,000 charging and discharging cycles [83].

Another research group from China and USA developed a ZIF-L MOF derived carbon coated with dual metal sulfide composite as electrode material for SC application. ZIF-L derived carbon framework act as a template where bi-metallic nanosphere was decorated on that through sulfurization reaction. The resulting C@MCo_2S_4 (M = Ni and Fe) composite combines the high electrical conductivity of the carbon network with the rich redox activity of ternary metal sulfides. The assembled ASC with C@MCo_2S_4 as the positive electrode and soybean derived AC as the negative electrode, the device exhibits an E_D of 45.9 Wh/kg at a P_D of 775 W/kg with stable cycle performance [84]. Zixin Jia and his group members rationale design a MOF derived $NiCo_2S_4/Co_3S_4$ nanocages featuring abundant heterogeneous interface for SC application. The ZIF-67 act as a sacrificial framework structure which convert as a

NiCo-LDH through Ni^{2+} etching process and then through sulfurization solvothermal reaction it convert as heterogeneous $NiCo_2S_4/Co_3S_4$ nanocages. Kinetic analysis of the prepared electrode material indicates dominant diffusion-controlled charge storage with significant capacitive contribution, reflecting fast ion/electron transport enabled by the heterointerfaces. When assembled into a HSC ($NiCo_2S_4/Co_3S_4$//AC) exhibits high E_D of 40.8 Wh/kg at 806 W/kg, retaining 88.3% capacitance after 10,000 cycles. The enhanced electrochemical performance is attributed to the synergy of low crystallinity, multiphase sulfide heterojunctions, and hollow porous architecture (Fig. 8(A–E)) [79].

In similar way, Limu et al. fabricated a core-shell type metal sulfides derived ZIF-67 directly grown on NF where $NiCo_2S_4$ honeycomb like nanosheet structure decorated with Co_9S_8 hollow nanoparticles. The prepared hierarchal core-shell nanostructure delivers aerial capacitance of 13.04 F cm^{-2} at 10 mA cm^{-2} retains 77 % of its capacitance at high current densities, and exhibits good cycling stability with 94 % retention after 6000 charge–discharge cycles [85]. L. Zhuang and his group members developed a spherical NiS_2/V_2O_3 (NS2VO) heterostructures by sulfurization of nanoflower like Ni/V-MOF under inert atmosphere at 500 °C for 2 h. The coexistence of two different phases (NiS_2/V_2O_3) are confirmed by XRD and XPS analysis. The morphological evolution of nanoflower structure to porous sphere morphology with hierarchal architecture was confirmed by SEM and TEM analysis. The prepared heterostructure delivers excellent electrochemical performance in both two electrode and three electrode configuration. The assembled ASC device with NS2VO (positive) and AC (negative) electrodes exhibits excellent cycle stability which 91.4% retention after 10,000 charging/discharging cycles and maintained 100% columbic efficiency throughout the cycling test [86].

The MOF-on-MOF also an effective approach to prepare the metal sulfides based nanostructures for SC application. Jiaxi Xu et al. fabricated core-satellite structure $Ni_3S_4@Co_3S_4$ where rhombic dodecahedral shape of ZIF-67 was grown on spherical Ni-MOF then it converted as a metal sulfides through sulfurization in the presence of thioacetamide. This method preserves the morphological nature of MOF architecture while improving the electrochemical activity. Electrochemically, the optimized $Ni_3S_4@Co_3S_4$ delivers a high specific capacity of 747.3C/g at 1 A/g and retains 77% at 10 A/g, indicating good rate capability [87]. Similar to that 3D interconnected based morphology was synthesized by Jiahui Zhao et al. The MOF derived NiS_2@carbon microsphere interconnected by in-situ grown carbon nanotubes (xNCC) was fabericated by sublimed sulfidation reaction. The 3D interconnected conductive network effectively reduces the agglomeration of NiS_2, buffers volume expansion and enhance the ion/electron transport. The aqueous ASC delivers stable wide potential window up to 1.6 V, delivering an E_D of 21.6 Wh/kg and excellent cycling durability with 94.8% capacitance retention after 10,000 continuous cycles [88]. Shuangxing Cui and his group members constructed a metal sulfids in situ grown NF through Co-MOF-74 self-sacrificial template approach. The prepared amorphous $CoMoS_4$ exhibits hollow tube arrays with self-assembled nanosheet surfaces grown directly on NF. This unique structure provides abundant redox active sites, electrolyte penetration, and reduced charge-transfer resistance. The $CoMoS_4$ on NF delivers an excellent areal capacitance of 7.01 F cm^{-2} at 2 mA cm^{-2}. Mechanistic investigations reveal that Mo- and S-doped amorphous CoOOH formed during cycling is the genuine active species responsible for energy storage. Furthermore, the assembled $CoMoS_4$//AC ASC device achieves good E_D with 91.39% retention after 10,000 charge/discharge cycles [89]. The comparative performance of metal sulfides and their composites is summarized in Table 2 and Table S1, while the performance of flexible SC devices is provided in Table S2.

Other than above mentioned research works, several other research groups worked on MOF derived metal sulfides and their composite for SC application. Jingjing Hu and co-workers developed a spherical flower-shaped B-Ni_xS_y/C electrode material to fabricate an ASC device. The developed device (B-Ni_xS_y/carbon//AC) delivered an excellent E_D of 29.7 Wh/kg at a P_D of 996.2 W/kg [95]. Yue Zhu et al. synthesized a pyridine-3,5-dicarboxylate-based Ni-MOF-derived $Ni_9S_8/Ni_{17}S_{18}$@C composite through pyrolysis under an Ar/H_2 atmosphere. The prepared electrode acted as the cathode, while PC served as the anode to fabricate an ASC, which exhibited an exceptional E_D of 58.88 Wh/kg at a P_D of 799.63 W/kg [96]. Jiahong Zheng and Yuhan Wang prepared a Co_x-$Ni_{1-x}S_2$ hierarchal microspheres through MOF derived approach which exhibits high C_s (1 A/g at 1243.69 F/g) and good cycle stability [97].

2.5. MOF derived transition metal phosphates and their composite for SC application

Transition metal phosphates (TMPs) possess unique properties for various functional applications. In particular, the polyanionic (PO_4^{3-}) framework in metal phosphates provides excellent chemical and thermal stability, making them attractive for a wide range of electrochemical energy-storage applications [98]. Furthermore, TMPs exhibit good electrical conductivity and electrochemical activity, making them promising positive-electrode materials for SC applications. To further improve their electrochemical performance, MOF-derived strategies have been widely used to engineer nanostructured TMPs, prepare ternary TMPs, form carbon-based composites with TMPs and enable in situ growth of TMPs on conductive substrates such as NF or CC. These approaches can tune the electronic structure of TMPs, expose abundant redox-active sites, and increase the accessible surface area, thereby enhancing the specific capacity and E_D of the electrode materials [99].

In this regards, Chunyan Li et al. fabricated a ternary metal phosphate nanostructure through sacrificial template derived approach. First they synthesized 3D porous ZnCo-MOF nanoarray grown on CC through hydrothermal approach and further, 2D/3D NiZnCo-LDH architecture through ion-exchange approach then it get phosphatized at mild temperature to form a NiZnCo-P nanoarray on CC. The phosphatized temperature changes from 300 to 700 °C to get optimized nanostructure. Among the different phosphroization temperature, 600 °C provides uniform hierarchical 2D-3D nanoarchitecture NiZnCo-P nanoarray on CC. This mild phosphorizetion technique preserves the interconnected 2D-3D nanoarchitecture while developing a rough, pore-rich surface beneficial for electrolyte penetration and redox accessibility. The optimized NiZnCo-P nanoarray on CC electrode delivers very high C_s (2816 F/g at 1 A/g) and good cycle stability in three electrode configuration. The fabricated ASC device using NiZnCo-P//Zn-modified carbon nanosheets provides high E_D 62.5 Wh/kg at 750 W/kg and cycle stability shows no abnormal changes in capacitance retentions during an initial cycles and it gradually decreased with respect to 89.5% C_s retention over 10,000 cycles [90].

Another research group from South Korea developed an in situ MOF derived Ni-Fe-P-C on electrospun hollow carbon nanofibers (HCNFs) as an electrode material for SC application. The Ni-Fe bimetallic MOF was grown on HCNFs and then phosphorized into MOF derived conductive Ni-Fe-P-C@HCNFs electrode. Compared to Ni–P–C@HCNFs, and Fe–P–C@HCNFs, the Ni-Fe-P-C@HCNFs electrode exhibits faradaic storage with much stronger kinetics and lower resistance. The optimized Ni-Fe-P-C@HCNFs delivers 1392 F/g at 1 A/g and 764 F/g at 10 A/g with 89% capacitance retention after 10,000 cycles. EIS analysis further confirmed low R_s and R_{ct} values (0.65 and 0.36 Ω) of Ni-Fe-P-C@HCNFs. The assembled ASC with Ni-Fe-P-C@HCNFs (positive) and Fe–P–C@HCNFs (negative) electrodes achieves high E_D of 62.7 Wh/kg at a P_D of 8238.2 W/kg and fabricated ASC exhibits excellent C_s retentions of 92.4% retention after 10,000 charging/discharging cycles [91]. Liu et al. prepared a MOF-derived bimetallic phosphide via an etching-assisted, low-temperature phosphorization strategy. A solvothermally synthesized NiMn-MOF using the H_2BDC organic linker was converted into NiMn-DH-y through KOH/ethanol etching, where y denotes the etching time. The resulting NiMn-DH-y nanosheets were then phosphorized at 400 °C for 2 h under a nitrogen atmosphere to obtain bimetallic $(Ni_{1-x}Mn_x)_2P$ phases. The different Ni and Mn ratio of

Table 2
Comparative analysis of MOF derived metal sulfides, phosphates, and their composites: synthesis methods and electrochemical parameters.

S.No	Type of MOF	MOF derived material	Synthesis method	Capacitance (Three Electrode)	Supercapacitor device	E_D Wh/kg & P_D W/kg	Cycle stability	Ref
1. 1	Cu-MOF	MWCNTs @ Ni_3S_2/Cu_xS	Solvothermal reaction	1388 F/g @1 A/g	SSC	211.8 & 1290.5	100 % - 15,000 cycles	[76]
2. 2	Ni-MOF	Ni_3S_4/CuS@p-MXene	In situ MOF growth + sulfurization	1917 F/g @1 A/g	ASC- Ni_3S_4/CuS@MXene//AC	87.6 & 775	91.2% −30,000 cycles	[77]
3. 3	Ni–Co MOF	N-doped porous multishell CuCoS@NiCoS	Solvothermal and hydrothermal sulferization	1259 F/g @ 0.5 A/g	ASC- N-doped CuCoS@NiCoS//AC	87.3 & 825	81.3% −8400 cycles	[78]
4. 4	Al-based MOF	a/c-Co(Al)S/NF	Solvothermal, Acid etching and sulferization	3981.78 F/g @ 1 A/g	ASC- Co_9S_8/Co_3S_4 heterophase/ NF//AC	77.1 & 800	87.4% - 10,000 cycles	[80]
5. 5	ZnCo-MOF	$ZnS/Co_3S_4/Ti_3C_2T_x$ MXene	Solvothermal and sulferization	2193.8 F/g @ 1 A/g	ASC- $ZnS/Co_3S_4/Ti_3C_2T_x$ MXene// AC	66.9 & 750	73.42 % - 6000 cycles	[81]
6. 6	Co-MOF	Co–Ni–S/CNTs composite spheres	In situ growth of co-mof on CNTs and sulferization	540.6 F/g @ 1 A/g	ASC- Co–Ni–S/CNTs//AC	63.5 & 800	83.0% −10 000 cycles	[82]
7. 7	Cu–Co MOF	$CuCo_2S_4@FeS_2$	Hydrothermal and sulferization	400.10C/g @1 A/g	ASC- $CuCo_2S_4@FeS_2$//AC	63.99 & 1125	90.01 % - 10,000 cycles	[83]
8. 8	ZIF-L (Co-based MOF)	$C@MCo_2S_4$ (M = Fe, Ni)	LDH growth, hydrothermal and sulferization	342.5 mAh g^{-1} @ 1 A/g	ASC- $C@MCo_2S_4$ (M = Fe, Ni)//PC	45.9 & 775	94% −1000 cycles	[84]
9. 9	ZIF-67	NiCo2S4/Co3S4	Co-precipitation and solovo-thermal	1860 F/g @ 1 A/g	ASC- NiCo2S4/Co3S4//N-rgo	40.8 & 8595.6	89.6% - 5000 cycles	[79]
10.	ZIF-67 (Co-MOF)	$NF/NiCo_2S_4/Co_9S_8$	Hydrothermal and sulferization	13.04 F/cm^2 @ 10 mA cm^{-2}	ASC- $NF/NiCo_2S_4/Co_9S_8$//Rgo	36.9 & 800	90 % - 6000 cycles	[85]
11. 10	Bimetallic Ni/V-MOF	NiS_2/V_2O_3 heterostructure	Hydrothermal, sulferization and calcination	1295 F/g @ 1 A/g	ASC- NiS_2/V_2O_3//AC	35.1 & 763.3	91.4 % - 10,000 cycles	[86]
12. 11	MOF-on-MOF Ni-MOF@Co-MOF	$Ni_3S_4@Co_3S_4$	Hydrothermal, Epidoxial growth and sulferization	1494.6 F/g @ 1 A/g	Ni3S4@Co3S4//AC HSC device	30.8 & 750	85.4%-5000 cycles	[87]
13. 13	Ni-MOF	NiS_2@C/CNTs	Solovothermal and calcination	1572 F/g @ 1 A/g	ASC: Ni2S@C/CNTs//AC	21.6 & 402	94.8% - 10,000 cycles	[88]
MOF derived metal phosphate and their composites								
14. 13	ZnCo-MOF	2D–3D NiZnCo-P nano-arrays/CC	Ion exchange or ethcing and phospherization	2816 F/g @ 1 A/g	ASC- 2D–3D NiZnCo-P//CC// Zn@CNS/CC	62.5 & 750	89.5% −10 000 cycles	[90]
15. 14	Ni–Fe MOF	(Ni-Fe)-P-C@HCNFs	Electrospinning, solovothermal and phospherization	1392 F/g @ 1 A/g	ASC-(Ni-Fe)-P-C@HCNFs//Fe-P-C@HCNFs	62.7 & 820.8	92.4 % −10 000 cycles	[91]
16. 18	Ni–Mn bimetal MOF	$(Ni_{0.93}Mn_{0.07})_2$P-18/CC	Solvothermal and phosphorization	1702.2 F/g @ 1 A/g	ASC- $(Ni_{0.93}Mn_{0.07})_2$P-18/CC//AC	59.83 & 750	95.5 % 5000 cycles	[92]
17. 15	Cu-MOF	Cu3P/Cu@NC	Co-precipitation and calcination	1200 F/g @ 1 A/g	ASC- Cu3P/Cu@NC//AC	45.5 & 800	87.1% - 5000 cycles	[93]
18. 16	Ni-MOF	NiP@encapsulated in carbon microspehere	Solvothermal and carbonization	1622 F/g @ 1 A/g	ASC- NiP@CMS//AC	47.46 & 0.397	89.6%-8000 cycles	[94]

*ASC-Asymmetric Supercapacitor, SSC- Symmetric Supercapacitor, CC- Carbon cloth, NF- Nickel Foram, E_D-Energy Density and P_D-Power Density.

prepared $(Ni_{1-x}Mn_x)_2P$ delivers different structural and electrochemical properties. Among different metal phosphate composite, $(Ni_{0.93}Mn_{0.07})_2P$-18 shows uniform distribution of nanosheet morphology with 20 nm thickness and 500 nm of lateral size in SEM/-TEM analysis. BET analysis of $(Ni_{0.93}Mn_{0.07})_2P$-18 shows mesoporosity (type-IV isotherm) and high specific surface area of 30.16 m^2/g $(Ni_{0.93}Mn_{0.07})_2P$-18 exhibits maximum C_s of 851.1C/g at 1 A/g and retained 84.87% after 5000 cycles, while the assembled ASC device ($(Ni_{0.93}Mn_{0.07})_2P$-18/CC//AC) achieved higher E_D of 59.83 Wh/kg at 750 W/kg P_D with 95.5% retention after 5000 cycles [92]. Hussain et al. used a MOF-to-phosphate conversion strategy to prepare electrode material for SC. The Cu-MOF prepared through slow evaporation crystal growth technique by 2-amino-terephtlaic acid as an organic linker which act as a both cu source and an in situ carbon precursor. Then prepared Cu-MOF was phosphorized in the presence of $NaH_2PO_2{\cdot}H_2O$ to form a Cu_3P/Cu@NC heterostructure. It exhibits fast charge transfer and high conductivity due to the heterointerfaces and the N-doped carbon matrix. Compared to pristine MOF, the MOF derived Cu_3P/Cu@NC exhibits markedly stronger redox features and longer discharge time at the same current density, indicating substantially higher charge storage. Electrochemical kinetic analysis of MOF derived phosphate shows mixed diffusion/surface controlled capacitance which helps sustain rate capability. An ASC device was fabricated with (Cu_3P/Cu@NC//carbon black) using PVA-KOH gel electrolyte which achieves wider potential window of 1.6V and delivered high E_D of 45.5 Wh/kg at 800 W/kg P_D [93].

In that similar way, Daping Hu and his group members designed a nickel phosphate encapsulated in carbon microspheres (Ni_2P@CM) derived from spherical Ni-MOF through phosphorization method. The resulting uniform carbon shell provides continuous electron transport and helps restrain electrode expansion during cycling. Compared to Ni-MOF and Ni@CM-900, the phosphorization temperature optimized Ni_2P@CM-900 provide exceptional C_s (1622 F/g at 1 A/g) and it also gives excellent rate capability (1136 F/g at 30 A/g). Furthermore, the assembled ASC device achieved a C_s of 135.4 F/g (0.5 A/g) and achieves high E_D value (47.46 Wh/kg) [94]. Honglong Qu et al. followed different MOF derived engineering approach to prepare self-supported metal phosphate on NF. The MOF-on-MOF strategy was implemented to grow a Co_2P/Ni_2P heterostructure on NF surface. First Ni-MOF nanosheets were directly grown on the NF through hydrothermal method followed by PBA deposited on Ni-MOF which form PBA/Ni-MOF/NF and then it phosphorized to convert MOF into Co_2P/Ni_2P/NF heterostructure. The SEM analysis of Co_2P/Ni_2P/NF confirm the scattered nanosheet of Ni_2P on cubic Co_2P which is preserved from the cubic morphology of PBA. The contact angle measurement of the optimized electrode (NCP-2) shows superhydrophilic nature, which supports faster electrolyte infiltration for higher charge storage. The NCP-2 delivers specific capacity of 5124.2 mF cm^{-2} at 1 mA cm^{-2} with 80.69% capacitance retention after 3000 cycles in three electrode configuration. EIS analysis confirmed the lower R_{ct} value of NCP-2 (1.59) which is much lower than the Ni_2P (2.10 Ω) and Co_2P (1.87 Ω). Finally, the fabricated NCP-2//AC ASC device delivers excellent E_D and P_D values with exceptional cycle stability [33].

In a comparable manner, another research group from China developed a hollow NiCoP/rGO composite, which delivered a high E_D of 60.6 Wh/kg at a P_D of 749 W/kg in a NiCoP/rGO-20//AC HSC device configuration [100]. A.M. Kale et al. convert a ZIF-67 MOF into Co_2P/Cu_3P through phosphorization at an optimum temperature. The fabricated ASC device with Co_2P/Cu_3P (positive) and O, N, S@AC (negative) achieves maximum E_D 37.3 Wh/kg at a P_D of 915 W/kg [101]. Yuhan Cui et al. synthesized GO/MXene@NiZrP where Zr based MOF (UIO-66) used as a precursor to prepare that composite. The fabricate ASC device with GO/MXene@NiZrP exhibits excellent cycle stability of 83.3% capacitance retention after 10,000 cycles [102]. The comparative performance of metal phosphates and their composites is summarized in Table 2 and Table S1, while the performance of flexible SC devices is provided in Table S2.

2.6. MOF derived carbon material for SC application

A carbon based materials have high specific surface area, electronic conductivity and exceptional chemical stability makes them promising candidate for the variety energy and environmental applications [103]. However, conventional synthetic strategies, including pyrolysis of organic precursors or biomass, vapor-phase decomposition, and high-temperature solvothermal or hydrothermal routes, often suffer from limited control over morphology, specific surface area, and particle size distribution. These intrinsic limitations restrict the full realization of electrochemical performance and impede a fundamental understanding of the underlying reaction mechanisms. Recently, 3D-MOF structures have been considered excellent precursors for the preparation of PC nanomaterials. By tuning the synthesis conditions of the MOF precursors and the pyrolysis temperature, the resulting porous structures and compositions can be effectively controlled [104].

Dongdong Huang et al. fabricated a MOF derived hierarchal carbon network as an electrode material for SC application. The p-π conjugated organic ligand synthesized through Schiff-base method which act as nitrogen doped and carbon enriched ligand for synthesis MOF and it further carbonized at different pyrolysis temperature to form hierarchal carbon network. Structural and morphological analysis confirm the controlled carbonization increase the degree of graphitization and active surface area while preserving the framework structure which leads to the improvement in the electrochemical performance. The optimized carbon material (MOF-B-600) delivers higher C_s 2727.5 F/g at 1 A/g. They developed aqueous ASC with MOF-B-600 (positive) and AC (negative) and it delivers maximum E_D of 63.62 Wh/kg at a P_D of 400 W/kg [105].

Similarly, another research group from china developed binary MOF (Zn/Mn-MOF) derived PC nanorods through pyrolysis and alkaline activation technique. Through controlled carbonization, acid etching, and KOH activation, hierarchical PC structures with ultrahigh specific surface area (~2020 m^2 /g) and optimized mesoporous architectures can be achieved, significantly enhancing electrolyte accessibility and charge transfer kinetics. The optimized PC nanorods electrode material (PCNR-2) delivers excellent C_s of 418 F/g with 99% capacitance retention after 10,000 charging-discharging cycles. The SSC device was built with PCNR-2 using 6M KOH as well as Et_4NBF_4/AN electrolytes and in both SC configuration delivers excellent C_s [106].

Mingliang He and his group members developed an in situ synthesis approach for developing a carbon based electrode material for SC. Initially, vertically aligned graphene (VG) was grown on CC via plasma-enhanced chemical vapor deposition (PECVD), followed by the growth of ZIF-67 on the VG-CC surface. During subsequent thermal treatment, the organic moieties of ZIF-67 were converted into CNTs, which were uniformly aligned on the VG-CC surface. This electrode preparation strategy reducing intrinsic limitations of conventional carbon electrode such as low wettability and less electro active interface. The resulting hybrid electrode exhibits enhanced hydrophilicity, enlarged effective surface area, and improved electron transport pathways, enabling efficient ion diffusion and charge storage. In electrochemical reactions, the incorporation of $[Fe(CN)_6]^{3-/4-}$ with KOH provides additional redox reaction, high areal capacitance (1526.5 mF /cm^2) with excellent columbic efficiency and cyclic stability over 10,000 cycles. Furthermore, the ASC device was fabricated with CNT-VG-CC (positive) and the EOVG-CC (negative) electrodes. The fabricated ASC device exhibits higher E_D 179.7 μW h/cm^2 at a P_D of 8000.0 μW/cm^2 (Fig S3 (A-C) [107].

Rui Miao et al. developed a Zn-BTC-derived PC material exhibiting solvent-tuned morphology control. When ethanol/water ratio varied from 0 to 100% during the synthesis, the morphology of Zn-BTC evolved from rod like structure to triangular structures, which was preserved after carbonization and alkaline etching, confirming the structural

inheritance characteristic of MOF-template carbons. Among the different synthesized PC, RTPC-50 (50% ethanol solvent) exhibits high specific surface area of 1930 m^2 /g and an average pore size of 2–3 nm, enabling efficient electrolyte ion accessibility and rapid charge transport. Electrochemical measurement reveals that the prepared electrode material exhibits high C_s of 287.2 F/g at 1 A/g with excellent rate capability. In SSC device configuration delivers high E_D of 16.09 Wh/kg at 698 W/kg P_D [108].

Guosai Jiang et al. studied a spherical porous carbon (SPC) derived from Mg-MOF through calcination and activation strategy. The spherical structure of Mg-MOF retained its morphology even after the high temperature calcination and activation which results SPC with particle size of 2-3 μm and exceptional specific surface area of 2175 m^2 /g. The porosity created through MgO removal and subsequent KOH activation is well visible in the SEM and TEM images which creates interconnected micro and mesoporous channels that facilitate efficient electrolyte ion diffusion. Raman spectroscopy indicated increased defect density after activation ($I_D/I_G = 1.03$), suggesting enhanced electrochemically active sites. In three electrode configuration, SPC delivers high C_s of 362.5 F/g at 1 A/g with excellent rate capability. The assembled SSC delivered a high energy density of 15.6 Wh/kg at a power density of 372.2 W/kg. The cycling stability test confirmed superior capacitance retention of 94.2% after 15,000 charge–discharge cycles (Fig. S4 (A-G)) [109].

Another research group from USA fabricated a Cu-MOF with polymer (PVA/PVP) composite derived hierarchical carbon network for SC application. To synthesis optimized carbon network, different weight ratios of MOF was used in polymer-MOF hydrogel preparation. The 3D polymer-MOF network facilitated strong interfacial interactions via hydrogen bonding and π–π stacking, which upon carbonization generated interconnected carbon frameworks with large accessible surface area (1707 m^2 /g) and continuous conductive pathways. The optimized CPM-25 electrode exhibited dominant EDLC behaviour with a high C_s of 385 F/g at 0.1 A/g and excellent rate capability, maintaining 303 F/g at 10 A/g due to rapid charge transfer kinetics and reduced internal resistance. The SSC assembled using CPM-25 electrodes delivered reasonable energy and power densities of 10.51 Wh/kg and 5.454 kW/kg, respectively. During cycling, the capacitance retention initially decreased within the first 1000 cycles, subsequently stabilized, and ultimately retained 90% of its initial capacitance after 10,000 cycles [110].

In a similar way, Park et al. developed a strategy for the controlled growth of PANI nanorods on KOH activated ZIF-8 derived nanoporous carbon (AZC), enabling synergistic integration of EDLC and faradaic charge-storage mechanisms. KOH activation nanoporous carbon have increased active surface area, good mesoporosity and providing numerous amount of active sites for the growth PANI nanorods. The BET surface area analysis confirm the specific surface of ZC (858.3 m^2/g) which was increased after the activation (AZC = 2688.4 m^2/g) and it results higher C_s of AZC. However, after coating PANI nanorods onto the surface of AZC (P-AZC), the specific surface area of P-AZC decreases, while the overall porosity of the material increases due to the highly porous nature of the PANI nanorods. The P-AZC exhibits higher C_s of 635.3 F/g, substantially exceeding that of pristine MOF-derived carbon electrodes and it also maintains 75% capacitance retention 5000 cycles. The estimated E_D and P_D of P-AZC are 79.3 Wh/kg and 500 W/kg, respectively [111].

Another research group from china fabricated a Zn-MOF-74 derived controlled nitrogen doped PC and analysed their electrochemical properties with 1-Ethyl-3-methylimidazolium tetrafluoroborate ($EMIMBF_4$ or EMIMTFSI) ionic liquid electrolyte. Structural characterization confirmed that urea functionalization successfully introduced nitrogen species without disrupting the parent MOF framework. The XPS analysis confirmed the presence of pyridinic-N, pyrrolic-N, and graphitic-N configurations in the nitrogen doped PC. The morphological analysis revealed that increase of urea content gradually transformed nanorod-assembled spherical structures into thinner nanowire networks, accompanied by a reduction in BET surface area from 2812 to 2160 m^2/g due to partial mesopore filling. The optimized Zn-MOF-74 derived carbons (ZMC-50) electrode exhibits maximum C_s of 108.02 F/g at 0.2 A/g which is much higher than the un-doped carbon electrode in the $EMIMBF_4$ electrolyte. In EMIMTFSI electrolyte, delivers slightly lower C_s due to the larger radius. The optimized electrode exhibited lower cycling performance with only 61% capacitance retention after 10,000 cycles and achieved a high E_D of 33.75 Wh/kg at 150 W/kg, maintaining 26.1 Wh/kg even at high P_D [112]. The comparative performance of porous carbon is summarized in Table 3 and Table S1, while the performance of flexible SC devices is provided in Table S2.

2.7. Comparative overview of different MOF derived nanostructure classes for high energy density supercapacitor

From the above discussion, MOF derived electrode materials for high E_D SC have been collectively and systematically analysed based on their material class, charge-storage behaviour, and device-level performance. MOF derived transition metal oxides and hydroxides generally exhibit excellent redox activity and high capacitance due to their multiple oxidation states; however, in some cases, their poor intrinsic conductivity, sluggish ion transport, and structural degradation during repeated charge–discharge cycles limit their device level energy density and cycling stability. MOF-derived sulfides usually possess higher electrical conductivity and richer redox activity than oxides, enabling high capacitance and improved rate performance. Nevertheless, their practical application can be restricted by phase transformation, volume expansion, surface oxidation, and partial dissolution of active species, which reduce long-term cycling stability and practical energy output. MOF derived phosphates can offer stable frameworks and multiple redox active centers, but their relatively poor intrinsic conductivity and the presence of electrochemically inactive phosphate groups may reduce charge-transfer efficiency and gravimetric capacitance. To overcome these limitations, several studies have incorporated carbon-based nanomaterials or MOF-derived porous carbon networks into transition metal compounds. These carbonaceous frameworks not only improve electrical conductivity and electron transfer but also buffer volume changes, prevent particle aggregation, enhance electrolyte accessibility, and shorten ion-diffusion pathways. Therefore, the rational integration of redox-active MOF-derived compounds with conductive porous carbon matrices is an effective strategy for achieving device level high energy density SCs with improved rate capability and cycling durability.

For an overall comparative evaluation, a Ragone plot was constructed to compare the E_D and P_D characteristics of different electrode materials with those of commercial energy-storage systems (Fig. S5). MOF-derived metal oxides, metal oxide/carbon composites, LDH-based composites, metal sulfides, metal phosphates, and porous carbon-based materials generally occupy an intermediate region between conventional capacitors and commercial Li-ion batteries, highlighting their potential for high-performance SC applications. Among these materials, hybrid composite electrodes typically exhibit improved energy density while maintaining acceptable power capability, which can be attributed to the synergistic effects of pseudocapacitive redox reactions, enhanced electrical conductivity, and improved ion/electron transport pathways. Based on reports published since 2021, several MOF-derived hybrid nanostructured composite electrode based SC devices have achieved energy densities exceeding 100 Wh kg^{-1}, approaching the lower energy-density range of commercial Li-ion batteries. However, further scientific and technological advancements are still required to improve scalability, cycling durability, electrode mass loading, device-level performance, and practical manufacturability before MOF-derived material-based SCs can be commercialized.

Table 3
Comparative analysis of MOF derived carbon and their composites: synthesis methods and electrochemical parameters.

S. No	Type of MOF	MOF derived material	Synthesis method	Capacitance (Three Electrode)	SC device	E_D Wh/kg & P_D W/kg	Cycle stability	Ref
1	Ni-MOF	Nitrogen doped hierarchical carbon	Solvothermal and calcination	2727.5 F/g @ 1 A/g	ASCs MOF-B-600 (Positive)//AC (Negative)	63.62 & 400	86.67% - 20,000 cycles	[105]
2	Zn/Mn-MOF-74	PC nanorods	Hydrothermal and carbonization	418 F/g @ 2 A/g	SSCs	30.0 & 17,000	99 % - 10,000 cycles	[106]
3	Zn-MOF	Rod-like PC	Hydrothermal and carbonization	287.2 F/g @ 1 A/g	SSCs	16.09 & 698	97.9% −200,000 cycles	[108]
4	Mg-BTC MOF	Spherical Activated PC	Solvothermal and carbonization	362.5 F/g @ 1 A/g	SSCs	15.6 & 372.2	66.6% −10,000 cycles	[109]
5	Ni-MOF	MOF-derived hierarchical PC network	Hydrothermal and calcination	385 F/g @ 0.1 A/g	_	13.3 & 5.454 (three electrode)	90% - 10,000 cycles	[110]
6	ZIF-8	P-AZC	Carbanization and in situ polymerization	635.3 F/g @ 5 mV / s	_	79.3 & 500 (three electrode)	75% after 5000 cycles	[111]
7	Zn-MOF-74	N-doped MOF-derived carbon	Hydrothermal and carbonization	108.02 F/g @ 0.2 A/g	_	26.1 & 3750 (three electrode)	61% −10,000 cycles	[112]

*ASC-Asymmetric Supercapacitor, SSC- Symmetric Supercapacitor, PC- porous carbon, P-AZC- PANI Nanorods Activated ZIF-8-derived carbon, E_D-Energy Density and P_D-Power Density.

2.8. DFT and In situ/operando analysis of MOF derived nanostructured materials

The results obtained from structural, morphological, and electrochemical characterizations of MOF and MOF derived nanostructured materials provide valuable insight into their overall electrochemical performance. However, to complement and rationalize the experimental findings, density functional theory (DFT) calculations are crucial. DFT offers atomic level understanding of the structural and electronic properties, charge-transfer behavior, and charge-storage mechanisms of electrode materials. In this context, band structure and binding energy calculations can support the interpretation of photoemission spectroscopy results, while DFT-simulated crystal structures can validate phase purity and structural transformations experimentally confirmed by XRD analysis. Moreover, DFT provides deeper insight into defect formation, including oxygen vacancies, metal–nonmetal bonding interactions, and local electronic redistribution. Density of states (DOS) analysis further elucidates the contribution of specific metal centers or active orbitals to redox activity, whereas work function analysis reveals the electron-donating or electron-withdrawing tendency of the material. Also it complement in situ/operando XRD, XPS, and Raman analyses by providing atomic level insights into phase transformations, interfacial bond rearrangements, and electronic structure changes under dynamic electrochemical cycling conditions. Therefore, such theoretical investigations are highly useful for understanding charge storage behaviour and guiding the rational design of efficient, high-performance SC electrode materials. For an example, DFT-based analysis revealed the facet-dependent charge-storage activity of MOF-derived α-NiS/rGO electrodes. The calculated surface energies for the α-NiS (110), (102), and (101) planes were 0.033, 0.069, and 0.086 eV Å, respectively, while the corresponding OH^- adsorption energies were 1.648, 3.101, and −0.879 eV. The (110) plane surface have unique nature of strong affinity towards OH- due to the high negative adsorption energy and shorter Ni-O bond length. These theoretical results agreed well with TEM observations showing abundant (101)/(110) edge exposure and explained the superior electrochemical performance of α-NiS/rGO [113]. In another work, DFT calculations confirmed strong interfacial coupling between NiCo-LDH and vertical graphene in the G-LDH@VG Mott–Schottky heterostructure. The increased electron density near the Fermi level and charge redistribution at the LDH/VG interface reduced the charge-transfer barrier, promoted electron transport, and supported the high areal capacitance of 5513.8 mF cm^{-2} with 82.1% rate capability [114]. E Torabi et al., reported MOF derived MnNi hydroxide based electrodes for SC approach and they did theoretical analysis using DFT-based quantum study. DFT analysis of $Mn(OH)_2$/$Ni(OH)_2$ showed strong electron density near the Fermi level, mainly from Mn 3d orbitals, leading to a high quantum capacitance of 4925 mF cm^{-2}. This theoretical result supports the excellent performance of MnNi-6, which delivered 4031.51 mF cm^{-2} and 86.34% retention after 10,000 cycles [115]. Similarly in another research work, DFT calculations showed that Nb/Co-NDPC has the most uneven electrostatic potential and strongest K^+ adsorption energy (−1.92 eV), indicating enhanced ion adsorption and EDLC formation. This supports its superior capacitance of 293 F g^{-1} at 0.5 A g^{-1} and 82% retention at 20 A g^{-1} [116]. Nwaji et al. reported defect-engineered MOF-derived Fe_3C@$NiCo_2S_4$ nanospike electrodes for hybrid SCs. DFT analysis revealed strong coupling between electrolyte OH^- oxygen and surface metal sites of FeCNiCoS, with a short OH^-–metal distance of 1.91 Å and favourable adsorption energy of −1.84 eV. This enhanced OH^- adsorption promoted faster redox kinetics, supporting the high specific capacitance of 1894.2 F g^{-1} at 1 A g^{-1} and 92.5% cycling retention [117]. To further correlate theoretical predictions with experimental observations, in situ/operando techniques provide real-time evidence of structural evolution, morphological reconstruction, and interfacial changes.

Xing et al. employed in situ heating TEM and synchrotron-based analysis to clarify the pyrolysis-driven structural evolution of ZIF-8-derived porous carbon. The in situ results revealed progressive framework shrinkage, Zn/N volatilization, and the persistence of atomically dispersed Zn–N_1 sites even at 1100 °C. Complementary DFT calculations showed that the asymmetric Zn–N_1 configuration exhibits stronger OH^- adsorption and higher electronic density near the Fermi level than Zn–N_4, indicating improved ion interaction and electrochemical activity. These combined in situ and theoretical insights explain the enhanced charge-storage behavior of PC-1100 in SC applications. In situ Raman analysis provides direct evidence of the redox evolution of electrode materials during electrochemical charging/discharging. For the CoNi$_3$Mn$_1$-OH/CC electrode, the Raman bands at ~550 and ~468 cm^{-1} gradually intensified during charging, confirming the oxidation of Ni^{2+}/Co^{2+} to Ni3+/Co3+ as the main charge-storage process. During discharge, these peaks weakened and nearly disappeared, indicating a reversible redox reaction. This real-time spectral response supports the CV/GCD results and confirms the stable pseudocapacitive behaviour of the trimetallic hydroxide electrode [118]. Operando electrochemical quartz crystal microbalance (EQCM) analysis was used to monitor real-time mass changes in $Ni_3(HITP)_2$ MOF electrodes during electrochemical charging/discharging. The reversible mass variation

confirmed that cation adsorption/desorption is the dominant charge-storage process, while anion contribution is relatively minor. This operando evidence provides direct insight into ion movement at the MOF–electrolyte interface and clarifies the capacitive charging mechanism of layered MOF SC electrodes [119]. In another research work, In situ Raman and XAS analyses were used to clarify the charge-storage mechanism of NiHAB conductive MOF electrodes in aqueous electrolyte. In situ Ni K-edge XAS showed no significant change in the Ni oxidation state, indicating that Ni sites are not directly involved in the redox process. These results confirm that NiHAB stores charge mainly through pH-dependent surface pseudocapacitance associated with the organic ligand framework [120]. In situ UV–Vis and Raman spectroelectrochemical analyses revealed that ZIF-67 undergoes significant structural reconstruction during electrochemical treatment. The original tetrahedral Co sites in ZIF-67 were progressively converted into α/β-Co $(OH)_2$ and subsequently oxidized to CoOOH, indicating that the in situ-formed cobalt oxyhydroxide species, rather than the pristine MOF metal nodes, act as the real active sites. The above section highlights the importance of in situ analysis for identifying electrochemically generated active phases in MOF-based electrodes [121]. In situ heating TEM and synchrotron analyses revealed the real-time structural evolution of ZIF-8-derived porous carbon, showing progressive Zn/N volatilization, framework shrinkage, and residual single Zn atoms stabilized as $Zn–N_1$ sites even at 1100 °C. DFT calculations further confirmed that the $Zn–N_1$ configuration has lower OH^- adsorption energy than $Zn–N_4$ and higher electronic density near the Fermi level, indicating improved ion interaction and electrochemical activity. These in situ and theoretical results explain the enhanced capacitance behaviour of PC-1100 in SC applications [122].

3. Conclusion and future perspective

In recent years, the development of various MOF derived transition metal compounds (such as oxides, hydroxides, sulfides, and phosphates), porous carbons and their composites as electrode materials has demonstrated high specific surface area, tunable pore architecture, and improved electrical conductivity. This review highlights how different synthesis strategies tune the morphological nature, structural characteristics, enhancing the electrochemical properties and provides a critical discussion of the electrochemical performance of the fabricated devices. However these MOF derived nanostructured material possess some common limitations such as slow charge-transfer kinetics, irregular pore size distribution, structural in-stability and difficult to do scalable synthesis. Although these materials often possess high surface area and well developed porosity, these features alone do not guarantee rapid electron transport, low charge-transfer resistance, or structural stability. Therefore, advanced characterization techniques and unique electrode fabrication procedure need to be developed and applied to gain an in-depth understanding of their charge-storage mechanisms.

To address these issues, synthesis conditions should be carefully controlled, particularly the heating rate, thermal-treatment temperature, and reaction atmosphere. Maintaining an appropriate inert atmosphere during thermal conversion is essential to preserve the porous framework, prevent excessive oxidation, and minimize structural collapse. In addition, conductive carbonaceous components such as graphene, CNTs, MXenes, or interconnected carbon networks can be incorporated into MOF-derived architectures to improve electrical conductivity, reduce charge-transfer resistance, and facilitate rapid ion transport. Recent studies have shown that the integration of MOF-derived metal oxides, sulfides, phosphates, and hydroxides with carbon nanomaterials can enhance structural stability and improve the utilization of redox-active sites, thereby increasing the E_D and cycling stability of fabricated SC devices [49,61,76,91]. More importantly, future research need to focus on designing single MOF precursors capable of generating both carbonaceous frameworks and metal-based nanostructures. Such an approach could provide a promising pathway for fabricating both positive and negative electrode materials from the same precursor system, thereby improving material compatibility, simplifying synthesis and advancing practical device fabrication.

A deeper understanding of metal–nonmetal interactions and the synergistic effects among multiple metal centers in complex ternary MOF-derived structures is essential for the rational design of high-performance SC electrode materials. However, the electrochemical charge storage mechanisms of these electrodes remain insufficiently understood. Therefore, the further development and application of advanced DFT techniques and in situ/operando characterization techniques, such as XPS, XRD, and XAFS, are highly essential for elucidating metal valence-state evolution, atomic level defects, interfacial structural changes, electrolyte-ion diffusion, and charge transfer pathways during the charge discharge processes of MOF-derived electrode materials.

Moreover, the widespread use of hydrothermal and solvothermal methods for MOF synthesis poses a major challenge for large scale production, which hinders their commercialization. Therefore, scalable synthesis strategies that preserve structural integrity are urgently needed. Accordingly, continuous flow [123], spray drying [124], continuous mechanochemistry [125], microwave-assisted flow [126], and electrochemical synthesis [127] approaches have been reported for the scalable production of MOFs such as HKUST-1, MOF-5, UiO-66, ZIF-8, Al-fumarate, Fe-MIL-53, MIL-100(Fe), and Cu-BTC. These techniques require further fine-tuning before they can be employed to fabricate MOF and MOF derived electrode materials for SC applications. Additionally, emerging artificial intelligence (AI) assisted approaches are gaining increasing attention in the design and synthesis of MOFs, as they can help predict optimized synthesis conditions, evaluate structural integrity, and reduce experimental trial-and-error. In particular, AI models can be developed to predict the optimal pyrolysis temperature for a given MOF topology, identify stable metal ratios in MOF-derived materials, screen favourable heteroatom dopants, and determine defect configurations that improve charge-storage kinetics and cycling stability. Such advances are expected to be highly beneficial for the development of efficient MOF-derived nanostructured electrode materials, ultimately enabling the fabrication of commercially viable SC devices.

Although the incorporation of insulating polymeric binders such as PVDF and PTFE in high-porosity MOF and MOF derived nanostructured electrodes ensures adequate mechanical stability and strong adhesion to the underlying current collector features that are advantageous for scalable manufacturing and it simultaneously imposes significant performance limitations. These include blockage of active sites, deterioration of electronic conductivity, restricted ion transport, and an increase in electrochemically inactive mass, all of which collectively diminish the gravimetric capacitance.

To address these limitations, recent studies have shown that binder-free electrode architectures have gained considerable attention as promising platforms for high-performance SCs. The in situ growth of MOF-derived nanostructures on conductive substrates such as NF, CC, and CW through hydrothermal/solvothermal synthesis, electrodeposition, and self-templated conversion approaches can enhance specific capacitance, cycling stability, and device-level energy density. In particular, self-standing films composed of MXene, CNT, or graphene integrated MOF-derived nanostructures are highly attractive for flexible and wearable energy-storage devices because they eliminate polymeric binders and reduce inactive electrode components. Among these, MXene based films are especially promising owing to their high electrical conductivity and layered ion-transport channels, which can lower interfacial resistance and facilitate electrolyte-ion diffusion. Therefore, systematic investigation and further optimization of such binder free hybrid architectures are crucial for advancing next-generation flexible SC devices.

Moreover, beyond the development of advanced positive and negative electrode materials, greater emphasis should be placed on complete device engineering, particularly through the rational selection of solid-

state and quasi-solid-state electrolytes. Such efforts are essential to improve the practical performance, mechanical reliability, safety, and long-term operational stability of fabricated SC devices. Continued progress in these directions will significantly accelerate the commercial translation of MOF derived material based SCs in the near future.

CRediT authorship contribution statement

P. Varatharajan: Conceptualization, Data curation, Formal analysis, Methodology, Validation, Visualization, Writing – original draft, Writing – review & editing. **Kumar Gokulkumar:** Data curation, Formal analysis, Resources, Software, Visualization, Writing – review & editing. **Shih-Hsuan Chen:** Data curation, Resources, Software, Validation, Visualization. **Neeraja Bose:** Data curation, Formal analysis, Software, Validation, Writing – review & editing. **Elango Kandasamy:** Conceptualization, Investigation, Project administration, Supervision, Validation, Writing – original draft, Writing – review & editing. **Kun-Mu Lee:** Conceptualization, Funding acquisition, Investigation, Project administration, Supervision, Validation, Writing – original draft, Writing – review & editing.

Declaration of competing interest

The authors declare that they have no known competing financial interests or personal relationships that could have appeared to influence the work reported in this paper.

Acknowledgments

The authors gratefully acknowledge financial support from the National Science and Technology Council (NSTC), Taiwan, under Project No. NSTC 111-2223-E-182-001-MY4. This research was also supported by the Chang Gung University, Taiwan. Project No (URRPD2R0011).

Appendix A. Supplementary data

Supplementary data to this article can be found online at https://doi.org/10.1016/j.jpowsour.2026.240526.

Data availability

Data will be made available on request.

References

[1] I. Pushparaj, A. Karuthedath Parameswaran, S.S. Srinivasan, M. Kiehbadroudinezhad, A. Merabet, H. Hosseinzadeh-Bandbafha, Review of latest advances and prospects of energy storage systems: considering economic, reliability, sizing, and environmental impacts approach, Cleanroom Technol. 4 (2022) 477–501, https://doi.org/10.3390/cleantechnol4020029, 4 (2022) 477–501.

[2] Handbook of Clean Energy Systems, Handb. Clean Energy Syst., 2015, https://doi.org/10.1002/9781118991978. WEBSITE:WEBSITE:PERICLES;JOURNAL:JOURNAL:MRWSERIES;ISPURCHASABLE:BOOLEAN:TRUE;PAGE:STRING:BOOK.

[3] L. Guo, P. Hu, H. Wei, Development of supercapacitor hybrid electric vehicle, J. Energy Storage 65 (2023) 107269, https://doi.org/10.1016/J.EST.2023.107269.

[4] Y.S. Lee, J.K. Alagarasan, K. Dasha Kumar, T. Ramachandran, H.J. Kim, M. S. Khan, Y. Anil Kumar, M. Lee, S.S. Kim, Redox behavior in hydrothermally synthesized thistle flower-like Co3O4–NiO-GO composite for advanced supercapacitor electrodes, J. Phys. Chem. Solid. 192 (2024) 112114, https://doi.org/10.1016/j.jpcs.2024.112114.

[5] Z. Dai, C. Peng, J.H. Chae, K.C. Ng, G.Z. Chen, Cell voltage versus electrode potential range in aqueous supercapacitors, Sci. Rep. 51 (5) (2015) 9854, https://doi.org/10.1038/srep09854, 2015.

[6] P. Varatharajan, M.H. Mamat, N. Vasimalai, U. Rajaji, T.Y. Liu, Hierarchical nanostructured Co0.5Mn0.5WO4 efficient electrode material for asymmetric supercapacitor application, J. Taiwan Inst. Chem. Eng. 163 (2024) 105649, https://doi.org/10.1016/j.jtice.2024.105649.

[7] S. Deka, Nanostructured Mixed Transition Metal Oxide Spinels for Supercapacitor Applications, vol. 45, 2016, pp. 1–5, https://doi.org/10.1039/c5dt05074j.

[8] M. Ramzan, U. Amara, M. Zia, U. Rehman, K. Mahmood, M. Hanif, S. Sirati, H. Muhammad, M. Rafiq, M. Ajmal, S. Qadir, Z. Ping, A roadmap to nickel-based bimetallic metal-organic frameworks for supercapacitor applications, Coord. Chem. Rev. 532 (2025) 216547, https://doi.org/10.1016/j.ccr.2025.216547.

[9] H.R. Khan, A.L. Ahmad, Journal of industrial and Engineering chemistry Supercapacitors : overcoming current limitations and charting the course for next-generation energy storage, J. Ind. Eng. Chem. 141 (2025) 46–66, https://doi.org/10.1016/j.jiec.2024.07.014.

[10] R.R. Salunkhe, Y.V. Kaneti, J. Kim, J.H. Kim, Y. Yamauchi, Nanoarchitectures for metal – organic framework-derived nanoporous carbons toward supercapacitor applications. https://doi.org/10.1021/acs.accounts.6b00460, 2016.

[11] P. Ruschhaupt, C. Guhrenz, P. Schlee, S. Pohlmann, A. Varzi, S. Passerini, A. Balducci, Development of a high-energy Electrical double-layer Capacitor Demonstrator with 5000 F in an Industrial Cell Format, vol.571, 2023, pp. 1–10, https://doi.org/10.1016/j.jpowsour.2023.233016.

[12] H. Niu, N. Zhang, Y. Lu, Z. Zhang, M. Li, J. Liu, N. Zhang, W. Song, Y. Zhao, Z. Miao, Strategies toward the development of high-energy-density lithium batteries, J. Energy Storage 88 (2024) 111666, https://doi.org/10.1016/j.est.2024.111666.

[13] X. Zhang, S. Zhang, Y. Tang, X. Huang, H. Pang, Recent advances and challenges of metal – organic framework/graphene-based composites, Compos. Part B. 230 (2022) 109532, https://doi.org/10.1016/j.compositesb.2021.109532.

[14] L. Zhang, F. Luo, C. Yang, H. Yu, K. Tao, Binder-Free metal–organic Framework-based core–shell Arrays for Supercapacitors, 2025, pp. 17400–17413, https://doi.org/10.1039/d5dt01533b.

[15] X. Zhuang, S. Zhang, Y. Tang, F. Yu, Z. Li, H. Pang, Recent progress of MOF/MXene-based composites : synthesis , functionality and application, Coord. Chem. Rev. 490 (2023) 215208, https://doi.org/10.1016/j.ccr.2023.215208.

[16] Z. Xie, W. Xu, X. Cui, Y. Wang, Recent Progress in Metal – Organic Frameworks and Their Derived Nanostructures for Energy and Environmental Applications, 2017, pp. 1645–1663, https://doi.org/10.1002/cssc.201601855.

[17] Z. Zhu, W. Hu, X. Wu, Q. Zhang, Y. Hu, Q. Yan, X. Wang, W. Yuan, In situ self-assembled macroporous interconnected nanosheet arrays of Ni-1,3,5-benzenetricarboxylate metal – organic framework on Ti mesh as high-performance oxygen evolution electrodes, J. Colloid Interface Sci. 639 (2023) 274–283, https://doi.org/10.1016/j.jcis.2023.02.079.

[18] A.A. Yadav, Y.M. Hunge, S. Majumder, A.H.I. Mourad, M.M. Islam, T. Sakurai, S. W. Kang, Multiplicative rGO/Cu-BDC MOF for 4-nitrophenol reduction and supercapacitor applications, J. Colloid Interface Sci. 677 (2025) 161–170, https://doi.org/10.1016/j.jcis.2024.08.060.

[19] D.D. Kachhadiya, Z.V.P. Murthy, Preparation and characterization of ZIF-8 and ZIF-67 incorporated poly(vinylidene fluoride) membranes for pervaporative separation of methanol/water mixtures, Mater. Today Chem. 22 (2021) 100591, https://doi.org/10.1016/j.mtchem.2021.100591.

[20] L.Z. Wu, X.Y. Zhou, P.C. Zeng, J.Y. Huang, M.D. Zhang, L. Qin, Hydrothermal synthesis of Ni(II) or Co(II)-based MOF for electrocatalytic hydrogen evolution, Polyhedron 225 (2022) 116035, https://doi.org/10.1016/J.POLY.2022.116035.

[21] W. Zhang, Z. Shahnavaz, X. Yan, X. Huang, S. Wu, H. Chen, J. Pan, T. Li, J. Wang, One-Step solvothermal synthesis of raspberry-like NiCo-MOF for high-performance flexible supercapacitors for a wide operation temperature range, Inorg. Chem. 61 (2022) 15287–15301, https://doi.org/10.1021/ACS.INORGCHEM.2C02916.

[22] X. Li, Z. Wu, X. Tao, R. Li, D. Tian, X. Liu, Gentle one-step co-precipitation to synthesize bimetallic CoCu-MOF immobilized laccase for boosting enzyme stability and Congo red removal, J. Hazard Mater. 438 (2022) 129525, https://doi.org/10.1016/J.JHAZMAT.2022.129525.

[23] A.A. Bhoite, K.V. Patil, R.S. Redekar, J.H. Jang, V.A. Sawant, N.L. Tarwal, Recent advances in Metal-Organic Framework (MOF) derived metal oxides and their composites with carbon for energy storage applications, J. Energy Storage 72 (2023) 108557, https://doi.org/10.1016/J.EST.2023.108557.

[24] L. Li, Y. Liang, Y. Liu, M. Wei, B. Wang, D. Wang, Facile preparation of MnO x catalysts derived from MOFs for efficient toluene Oxidation : synergistic enhancement of active site density and reactivity, Sep. Purif. Technol. 363 (2025) 132214, https://doi.org/10.1016/j.seppur.2025.132214.

[25] J.F. Qin, M. Yang, T.S. Chen, B. Dong, S. Hou, X. Ma, Y.N. Zhou, X.L. Yang, J. Nan, Y.M. Chai, Ternary metal sulfides MoCoNiS derived from metal organic frameworks for efficient oxygen evolution, Int. J. Hydrogen Energy 45 (2020) 2745–2753, https://doi.org/10.1016/j.ijhydene.2019.11.156.

[26] M. Liu, Y. Zhang, A. Cheng, L. Zhu, L. Xie, Q. Han, X. Qiu, Y. Xiao, X. Cao, Micron-flower MOF-derived cobalt–nickel phosphate as high-performance anodes for Li-storage systems, Chem. Eng. J. 498 (2024) 155639, https://doi.org/10.1016/j.cej.2024.155639.

[27] Z. Jin-Da, L. Li-Bing, Y. Ze-Qing, High energy density supercapacitor electrode materials based on mixed metal MOF and its derived C@bimetal hydroxide embedded onto porous support, Synth. Met. 277 (2021) 116775, https://doi.org/10.1016/j.synthmet.2021.116775.

[28] L. Zhang, H. Yu, K. Tao, Vacancy engineering of metal-organic framework-derived nickel - cobalt- manganese layered double hydroxide cathode and Bi 2 O 3 anode for aqueous alkaline batteries, J. Energy Storage 150 (2026) 120474, https://doi.org/10.1016/j.est.2026.120474.

[29] Y.C. Wang, W.B. Li, L. Zhao, B.Q. Xu, MOF-derived binary mixed metal/metal oxide @carbon nanoporous materials and their novel supercapacitive performances, Phys. Chem. Chem. Phys. 18 (2016) 17941–17948, https://doi.org/10.1039/C6CP02374F.

[30] J. Liu, C. Meng, Q. Liu, N. Li, R. Yu, M. Zeng, Fire-resistant iron-based phosphates/phosphorus-doped carbon composites derived from phytic acid-

treated metal organic frameworks as high-efficiency microwave absorbers, Carbon N. Y. 200 (2022) 472–482, https://doi.org/10.1016/j.carbon.2022.08.037.
[31] W. Sun, X. Tao, P. Du, Y. Wang, Carbon-coated mixed-metal sulfide hierarchical structure: MOF-derived synthesis and lithium-storage performances, Chem. Eng. J. 366 (2019) 622–630, https://doi.org/10.1016/j.cej.2019.01.178.
[32] Q. Han, W. Zhang, L. Zhu, M. Liu, C. Xia, L. Xie, X. Qiu, Y. Xiao, L. Yi, X. Cao, MOF-Derived bimetallic selenide CoNiSe2 nanododecahedrons encapsulated in porous carbon matrix as advanced anodes for lithium-ion batteries, ACS Appl. Mater. Interfaces 16 (2024) 6033–6047, https://doi.org/10.1021/acsami.3c18236.
[33] H. Qu, K. Liu, Q. Li, T. Cao, G. Chen, H. Guan, C. Dong, Z. Yin, MOF-on-MOF derived Co2P/Ni2P heterostructures for high-performance supercapacitors, J. Phys. Chem. Lett. 15 (2024) 10181–10189, https://doi.org/10.1021/acs.jpclett.4c02521.
[34] Y.V. Kaneti, J. Tang, R.R. Salunkhe, X. Jiang, A. Yu, K.C. Wu, Y. Yamauchi, Nanoarchitectured Design of Porous Materials and Nanocomposites from Metal-Organic Frameworks, 2017, https://doi.org/10.1002/adma.201604898.
[35] J. Song, L. Chai, M. Zhao, Y. Sun, X. Li, J. Pan, Research progress on metal organic framework derived porous carbon though interfacial engineering and synergistic effect, J. Power Sources 604 (2024) 234471, https://doi.org/10.1016/j.jpowsour.2024.234471.
[36] J. Jeon, R. Sharma, P. Meduri, B.W. Arey, H.T. Schaef, J.L. Lutkenhaus, J. P. Lemmon, P.K. Thallapally, M.I. Nandasiri, B.P. Mcgrail, S.K. Nune, In Situ One-step Synthesis of Hierarchical Nitrogen-Doped Porous Carbon for High-Performance Supercapacitors, 2014.
[37] J. Gu, L. Sun, Y. Zhang, Q. Zhang, X. Li, H. Si, Y. Shi, C. Sun, Y. Gong, Y. Zhang, MOF-derived Ni-doped CoP@C grown on CNTs for high-performance supercapacitors, Chem. Eng. J. 385 (2020) 123454, https://doi.org/10.1016/j.cej.2019.123454.
[38] C. Wang, Q. Yang, Y. Liu, L. Sun, R. Luo, W. Shi, MOF-derived anion exchange induced 2D/2D CF@CoS2/Co3O4/CNFs for ultra-long stable asymmetric supercapacitors, Colloids Surfaces A Physicochem. Eng. Asp. 656 (2023) 130458, https://doi.org/10.1016/j.colsurfa.2022.130458.
[39] N. Salandari-Jolge, A.A. Ensafi, B. Rezaei, Metal–organic framework derived metal oxide/reduced graphene oxide nanocomposite, a new tool for the determination of dipyridamole, New J. Chem. 45 (2021) 2781–2790, https://doi.org/10.1039/d0nj05329e.
[40] Sandwich-like reduced graphene oxide wrapped MOF-derived ZnCo 2 O 4 –ZnO–C on nickel foam as anodes for high performance lithium ion batteries - journal of Materials Chemistry A (RSC Publishing) DOI:10.1039/C5TA05733G, (n.d.). https://pubs.rsc.org/en/content/articlehtml/2015/ta/c5ta05733g (accessed March 4, 2026).
[41] N. Kitchamsetti, D. Kim, High performance hybrid supercapacitor based on hierarchical MOF derived CoFe2O4 and NiMn2O4 composite for efficient energy storage, J. Alloys Compd. 959 (2023) 170483, https://doi.org/10.1016/j.jallcom.2023.170483.
[42] P. Varatharajan, N. Vasimalai, Hierarchically grown ternary metal oxide nanocomposite on nickel foam for high energy density asymmetric supercapacitor applications, J. Energy Storage 142 (2026) 119565, https://doi.org/10.1016/j.est.2025.119565.
[43] Y. Chen, C. Kang, L. Ma, L. Fu, G. Li, Q. Hu, Q. Liu, MOF-derived Fe2O3 decorated with MnO2 nanosheet arrays as anode for high energy density hybrid supercapacitor, Chem. Eng. J. 417 (2021) 129243, https://doi.org/10.1016/j.cej.2021.129243.
[44] C. Shu, W. Chen, M. He, F. Yu, Y. Han, Metal–Organic framework-derived hierarchically heterostructured ZnCo2O4/ZnO composites for high-performance supercapacitors, Langmuir 41 (2025) 22481–22491, https://doi.org/10.1021/acs.langmuir.5c02914.
[45] A.M. Shahul Hameed, G. Shanmugam, E. Thirugnanasambandam, S. Kamaraj, Tweaking the efficiency of asymmetric hybrid supercapacitors with mechanochemically synthesized Mixed-Metal–Organic framework-derived metal oxides, Energy Technol. 12 (2024) 2301633, https://doi.org/10.1002/ente.202301633.
[46] I. Hussain, S. Sahoo, T. Hussain, M. Ahmad, M.S. Javed, C. Lamiel, S. Gu, T. Kaewmaraya, M.S. Sayed, K. Zhang, Theoretical and experimental investigation of in situ grown MOF-Derived oriented zr-mn-oxide and solution-free CuO as hybrid electrode for supercapacitors, Adv. Funct. Mater. 33 (2023) 2210002, https://doi.org/10.1002/adfm.202210002.
[47] H. Ju, Q. Tang, Y. Xu, X. Bai, C. Pu, T. Liu, S. Liu, L. Zhang, Prussian blue analogue-derived hollow metal oxide heterostructure for high-performance supercapacitors, Dalton Trans. 52 (2023) 12948–12957, https://doi.org/10.1039/d3dt01966g.
[48] A. Kumar, B.K. Satpathy, P. Goyal, R. Upadhyay, M.R.A. Kiapi, K. Jasuja, D. Menon, S.K. Misra, Bimetallic MOF-derived CuO-Co3O4 heterostructures as high-capacity electrodes for asymmetric supercapacitors, Chem. Eng. J. 520 (2025) 165685, https://doi.org/10.1016/j.cej.2025.165685.
[49] J. Pan, S. Li, F. Li, T. Yu, Y. Liu, L. Zhang, L. Ma, M. Sun, X. Tian, The NiFe2O4/NiCo2O4/GO composites electrode material derived from dual-MOF for high performance solid-state hybrid supercapacitors, Colloids Surfaces A Physicochem. Eng. Asp. 609 (2021) 125650, https://doi.org/10.1016/j.colsurfa.2020.125650.
[50] L. Zheng, S. Gao, S. Yao, Y. Huang, S. Zhai, J. Hao, X. Fu, Q. An, Z. Xiao, N-doped porous carbon with ZIF-67-derived CoFe2O4-Fe particles for supercapacitors, J. Colloid Interface Sci. 674 (2024) 735–744, https://doi.org/10.1016/j.jcis.2024.06.209.
[51] D.P. Hanamantrao, K. Kasiviswanathan, L. Kumaresan, S.R. Sasirajan Littleflower, S. Ramakrishnan, B. Rangasamy, K. Vediappan, Ultrahigh faradaic NiO anchored carbon-coated Fe-MOF derived Fe3O4 NiO-C@Fe3O4 as potential electrode for pouch-type asymmetric supercapacitor, J. Energy Storage 91 (2024) 112118, https://doi.org/10.1016/j.est.2024.112118.
[52] N. Kitchamsetti, D. Kim, A facile method for synthesizing MOF derived ZnCo2O4 particles on MXene nanosheets as a novel anode material for high performance hybrid supercapacitors, Electrochim. Acta 441 (2023) 141824, https://doi.org/10.1016/j.electacta.2023.141824.
[53] A. Mateen, M.S. Javed, S. Khan, A. Saleem, M.K. Majeed, A.J. Khan, M.F. Tahir, M.A. Ahmad, M.A. Assiri, K.Q. Peng, Metal-organic framework-derived walnut-like hierarchical Co-O-nanosheets as an advanced binder-free electrode material for flexible supercapacitor, J. Energy Storage 49 (2022) 104150, https://doi.org/10.1016/j.est.2022.104150.
[54] X. Sun, S. Wu, L. Chen, Q. Tong, L. Han, P. Wan, Y. Sun, L. Wang, Q. Yang, The construction of high-performance asymmetric supercapacitors by Bi-MOF-derived carbon skeleton with in situ activated Bi2O3/C and B-rGO/amorphous NiCoB, Chem. Eng. J. 522 (2025) 167546, https://doi.org/10.1016/j.cej.2025.167546.
[55] X. Yin, H. Li, R. Yuan, J. Lu, Hierarchical self-supporting sugar gourd-shape MOF-derived NiCo2O4 hollow nanocages@SiC nanowires for high-performance flexible hybrid supercapacitors, J. Colloid Interface Sci. 586 (2021) 219–232, https://doi.org/10.1016/j.jcis.2020.10.086.
[56] Y. Li, H. Xie, J. Li, Y. Yamauchi, J. Henzie, Metal-Organic framework-derived CoO x/Carbon composite array for high-performance supercapacitors, ACS Appl. Mater. Interfaces 13 (2021) 41649–41656, https://doi.org/10.1021/acsami.1c10998.
[57] D. Acharya, I. Pathak, B. Dahal, P.C. Lohani, R.M. Bhattarai, A. Muthurasu, T. Kim, T.H. Ko, K. Chhetri, H.Y. Kim, Immoderate nanoarchitectures of bimetallic MOF derived Ni–Fe–O/NPC on porous carbon nanofibers as freestanding electrode for asymmetric supercapacitors, Carbon N. Y. 201 (2023) 12–23, https://doi.org/10.1016/j.carbon.2022.08.091.
[58] S. Silambarasan, M. Sivakumar, K.R. Kumar, Z. Jiang, T. Maiyalagan, Nickel-doped Co3O4 spinel nanospheres embedded in nitrogen-doped carbon composites derived from bimetallic NiCo metal-organic framework as a high-performance asymmetric supercapacitor, New J. Chem. 47 (2023) 8649–8660, https://doi.org/10.1039/d3nj00517h.
[59] L. Han, X. Liu, Y. Chen, Z. Cui, Y. Hua, C. Wang, X. Zhao, X. Liu, High energy density pouch-type supercapacitor achieved by MOFs derived 3D hollow N-doped carbon with Fe 2 O 3 and hierarchical CuCo 2 S 4 @ NiFe-LDH core-shell nanostructures, Electrochim. Acta 467 (2023) 143131, https://doi.org/10.1016/j.electacta.2023.143131.
[60] M.B. Poudel, P.C. Lohani, D. Acharya, D.R. Kandel, A.A. Kim, D.J. Yoo, MOF derived hierarchical ZnNiCo-LDH on vapor solid phase grown CuxO nanowire array as high energy density asymmetric supercapacitors, J. Energy Storage 72 (2023) 108220, https://doi.org/10.1016/j.est.2023.108220.
[61] M. Lu, Y. Dong, Y. Wang, L. Shi, X. Xu, J. Zhou, G.S. Wang, Solvent-mediated synthesis of mesoporous ZnCo-ZIF derived ZnCoNi LDH@MXene for high-performance supercapacitors, Inorg. Chem. Front. (2025), https://doi.org/10.1039/d5qi01844g.
[62] J. Yuan, Y. Li, G. Lu, Z. Gao, F. Wei, J. Qi, Y. Sui, Q. Yan, S. Wang, Controlled synthesis of flower-like hierarchical NiCo-Layered double hydroxide integrated with metal-organic framework-derived co@c for supercapacitors, ACS Appl. Mater. Interfaces 15 (2023) 36143–36153, https://doi.org/10.1021/acsami.3c05061.
[63] D. Acharya, I. Pathak, A. Muthurasu, R.M. Bhattarai, T. Kim, T.H. Ko, S. Saidin, K. Chhetri, H.Y. Kim, In situ transmogrification of nanoarchitectured Fe-MOFs decorated porous carbon nanofibers into efficient positrode for asymmetric supercapacitor application, J. Energy Storage 63 (2023) 106992, https://doi.org/10.1016/j.est.2023.106992.
[64] D. Khalafallah, Y. Zhang, Q. Zhang, MOF−Derived Core-Shell La(OH)3@Cu(OH)2/Co(OH)2 heterostructure for supercapacitors, Batter. Supercaps 8 (2025), https://doi.org/10.1002/batt.202400497.
[65] W. Cao, W. Zhao, C. Xiong, Q. Long, N. Chen, G. Du, NiCo-MOF derived nanostructured NiCo-LDH@Ni(OH)2 heterogeneous composite as electrode material for hybrid supercapacitors, J. Energy Storage 64 (2023) 1–9, https://doi.org/10.1016/j.est.2023.107213.
[66] K.C. Lee, Y.S. Hsiao, M.Y. Sung, Y.L. Chen, N.J. Wu, J.H. Huang, E.C. Cho, H. C. Weng, S.C. Hsu, MOF-derived spinel NiMn2O4/CoMn2O4 heterojunction and its application in a high-performance photocatalyst and supercapacitor, J. Environ. Chem. Eng. 11 (2023) 110762, https://doi.org/10.1016/j.jece.2023.110762.
[67] W.W. Song, B. Wang, X.M. Cao, Q. Chen, Z.B. Han, ZIF-67-derived NiCo2O4@Co2P/Ni2P honeycomb nanosheets on carbon cloth for high-performance asymmetric supercapacitors, Inorg. Chem. Front. 8 (2021) 5100–5112, https://doi.org/10.1039/d1qi00934f.
[68] R. Bhosale, S. Bhosale, R. Sankannavar, V. Chavan, C. Jambhale, H. Kim, S. Kolekar, Bimetallic MnFe2-MOF and its derived MnFe2O4 nanostructures for supercapacitive applications, ACS Appl. Nano Mater. 7 (2024) 4078–4091, https://doi.org/10.1021/acsanm.3c05645.
[69] J. Zhang, T. Xie, M. Zhao, Y. Liu, N.D. Hoa, A.A. Kasera, R. Zeng, G. Ma, Y. Luo, Y. Wu, X. Lin, Mixed metal-organic framework-derived NiO/V2O3/C heterojunction nanostructures for high-performance hybrid supercapacitors, Electrochim. Acta 529 (2025) 146334, https://doi.org/10.1016/j.electacta.2025.146334.
[70] A.M. Ghadimi, S. Ghasemi, A. Omrani, F. Mousavi, Nickel Cobalt LDH/Graphene Film on nickel-foam-supported Ternary Transition Metal Oxides for

Supercapacitor Applications, vol. 37, 2023, pp. 3121–3133, https://doi.org/10.1021/acs.energyfuels.2c03040.
[71] L. Naderi, S. Shahrokhian, Wire-type flexible micro-supercapacitor based on MOF-assisted sulfide nano-arrays on dendritic CuCoP and V2O5-polypyrrole/nanocellulose hydrogel, Chem. Eng. J. 476 (2023) 146764, https://doi.org/10.1016/j.cej.2023.146764.
[72] K. Subbiramaniyan, R.J. Chung, B.J. Pan, S. Yougbaré, Y.F. Wu, L.Y. Lin, Constructing metal organic framework derived manganese cobalt layered double hydroxide nanosheets on Ni foam as cost-effective binder-free electrodes of high-performance supercapacitors, Mater. Today Chem. 33 (2023), https://doi.org/10.1016/j.mtchem.2023.101719.
[73] Z. Li, M. Yao, Z. Hu, L. Zhang, S. Gou, H. Feng, Y. Yang, X. Lu, g-C3N4 promoted NiFe-LDH self-assemble high performance supercapacitor composites, J. Alloys Compd. 919 (2022) 165805, https://doi.org/10.1016/j.jallcom.2022.165805.
[74] N. Ye, F. Luo, Y. Wang, L. Han, K. Tao, Construction of V-doped Co 9 S 8 nanoarrays as efficient free-standing electrodes for supercapacitor and oxygen evolution reaction, Int. J. Hydrogen Energy 166 (2025) 151014, https://doi.org/10.1016/j.ijhydene.2025.151014.
[75] Y. Gu, F. Cao, Y. Wang, C. Yang, X. Zhu, S. Xie, M. Chen, R. Liu, Metal-organic framework-derived transition metal sulfides promote the development of high-performance supercapacitors, J. Energy Storage 140 (2025) 119008, https://doi.org/10.1016/J.EST.2025.119008.
[76] Y. Abbasi, F. Jalali, S. Sheikhi, Preparation of nickel/copper sulfides from metal-organic frameworks. Applications to energy storage in a symmetric supercapacitor and electrocatalytic methanol oxidation, J. Alloys Compd. 938 (2023) 168450, https://doi.org/10.1016/j.jallcom.2022.168450.
[77] H. Guo, J. Zhang, F. Yang, M. Wang, T. Zhang, Y. Hao, W. Yang, Sandwich-like porous MXene/Ni3S4/CuS derived from MOFs as superior supercapacitor electrode, J. Alloys Compd. 906 (2022) 163863, https://doi.org/10.1016/j.jallcom.2022.163863.
[78] S. Yu, J. Xu, C. Xiang, Y. Zou, Z. Hu, F. Xu, L. Sun, Bifunctional metal-organic framework-derived nitrogen-doped porous multishell CuCoS@NiCoS nanospheres for supercapacitors and hydrogen evolution reactions, J. Energy Storage 55 (2022) 105541, https://doi.org/10.1016/j.est.2022.105541.
[79] Z. Jia, Y. Wang, J. Chen, Z. Cao, S. Pan, Y. Zhou, J. Sun, J. Zhu, X. Wang, Y. Fu, Metal-organic frameworks derived low-crystalline NiCo2S4/Co3S4 nanocages with dual heterogeneous interfaces for high-performance supercapacitors, Chin. Chem. Lett. 34 (2023) 107137, https://doi.org/10.1016/j.cclet.2022.01.030.
[80] M. Liao, K. Zhang, C. Luo, H. Zeng, Al-Based MOF-Derived Amorphous/Crystalline heterophase cobalt sulfides as high-performance supercapacitor materials, Inorg. Chem. 63 (2024) 14074–14085, https://doi.org/10.1021/acs.inorgchem.4c01881.
[81] L. Liu, W. Zhang, Y. Hao, Y. Zheng, L. Xiao, X. Yang, W. Feng, Y. Zhan, X. Guo, P. Feng, MOF-derived nanoflower-like ZnS/Co_3S_4/$Ti_3C_2T_x$ MXene: a binder-free electrode for high-performance asymmetric supercapacitors, J. Alloys Compd. 1042 (2025) 183900, https://doi.org/10.1016/j.jallcom.2025.183900.
[82] Z. Ma, R. Zheng, Y. Liu, Y. Ying, W. Shi, Carbon nanotubes interpenetrating MOFs-derived Co-Ni-S composite spheres with interconnected architecture for high performance hybrid supercapacitor, J. Colloid Interface Sci. 602 (2021) 627–635, https://doi.org/10.1016/j.jcis.2021.06.027.
[83] P. Naveenkumar, M. Maniyazagan, N. Kang, H.W. Yang, S.J. Kim, MoF-derived CuCo2S4@FeS2 nanohybrids for supercapacitor applications, Electrochim. Acta 513 (2025) 145546, https://doi.org/10.1016/j.electacta.2024.145546.
[84] X. Pang, J. Yu, Q. Yin, D. Chen, H. Dong, Q. Zhang, J. Sui, L. Sui, L. Dong, MOF derived hierarchical carbon-enhanced MCo2S4 for high-performance hybrid supercapacitors, Diam. Relat. Mater. 120 (2021) 108673, https://doi.org/10.1016/j.diamond.2021.108673.
[85] G.B. Lemu, W. Liu, X. Li, NiCo2S4 nanosheet/Co9S8 hollow nanoparticle derived from MOF hierarchical core/shell electrode material for supercapacitor applications, J. Mater. Sci. 59 (2024) 188–205, https://doi.org/10.1007/s10853-023-09187-8.
[86] L. Zhuang, J. Zhang, Y. Liu, G. Ma, C. Lin, Y. Wu, X. Lin, MOF-derived NiS2/V2O3 spherical heterostructures for high-performance supercapacitors, J. Phys. Chem. Solid. 209 (2026) 113237, https://doi.org/10.1016/j.jpcs.2025.113237.
[87] J. Xu, H. Guo, M. Wang, Y. Hao, J. Tian, H. Ren, Y. Liu, B. Ren, W. Yang, Hollow Ni3S4@Co3S4 with core-satellite nanostructure derived from metal-organic framework (MOF)-on-MOF hybrids as an electrode material for supercapacitors, Dalton Trans. 53 (2024) 4479–4491, https://doi.org/10.1039/d3dt04038k.
[88] J. Zhao, M. Wang, S. Wang, S. Zhang, J. Wang, X. Qiao, J. Mi, M. Ge, Y. Feng, MOF-derived NiS2@carbon microspheres wrapped with carbon nanotubes for high cycle performance supercapacitors, Electrochim. Acta 464 (2023) 142920, https://doi.org/10.1016/j.electacta.2023.142920.
[89] S. Cui, Y. Tang, W. Cui, G. Li, X. Xiao, K. Tao, L. Han, Self-sacrificing MOF-74 to amorphous CoMoS4 hollow tube with nanosheet surface for high stability supercapacitors, J. Alloys Compd. 1003 (2024) 175709, https://doi.org/10.1016/j.jallcom.2024.175709.
[90] C. Li, J. Wang, Y. Yan, P. Huo, X. Wang, MOF-derived NiZnCo-P nano-array for asymmetric supercapacitor, Chem. Eng. J. 446 (2022) 137108, https://doi.org/10.1016/j.cej.2022.137108.
[91] K. Chhetri, T. Kim, D. Acharya, A. Muthurasu, B. Dahal, R.M. Bhattarai, P. C. Lohani, I. Pathak, S. Ji, T.H. Ko, H.Y. Kim, Hollow carbon nanofibers with inside-outside decoration of Bi-metallic MOF derived Ni-Fe phosphides as electrode materials for asymmetric supercapacitors, Chem. Eng. J. 450 (2022) 138363, https://doi.org/10.1016/j.cej.2022.138363.
[92] S. Liu, W. Xu, K. Feng, X. Shi, C. Wang, Bimetallic MOF derived ni[sbnd]mn phosphide for high-performance supercapacitor electrode material, J. Energy Storage 96 (2024) 112684, https://doi.org/10.1016/j.est.2024.112684.
[93] N. Hussain, Z. Abbas, S.N. Ansari, G. Kedarnath, S.M. Mobin, Phosphorization engineering on a MOF-Derived metal phosphide heterostructure (Cu/Cu3P@NC) as an electrode for enhanced supercapacitor performance, Inorg. Chem. 62 (2023) 17083–17092, https://doi.org/10.1021/acs.inorgchem.3c01440.
[94] D. Hu, Y. Jia, F. Huang, Y. Long, C. Ai, P. Du, Nanoscale nickel phosphide encapsulated in carbon microsphere from a spherical MOF toward high-performance supercapacitors, J. Alloys Compd. 935 (2023) 168088, https://doi.org/10.1016/j.jallcom.2022.168088.
[95] J. Hu, Y. Shi, L. Sun, F. Xie, K. Gao, Y. Qu, H. Tan, Y. Zhang, MOF-derived spherical NixSy/carbon with B-doping enabling high supercapacitive performance, J. Mater. Sci. Technol. 153 (2023) 219–227, https://doi.org/10.1016/j.jmst.2022.11.065.
[96] Y. Zhu, S. Li, N. Fu, H. Wang, D. Tian, Y. Zheng, J. Wang, C. Zhang, S. Mu, J. Luo, Ni9S8/Ni17S18@C nanocrystals derived by Ni-MOF precursor for high-performance hybrid supercapacitor applications, J. Electroanal. Chem. 957 (2024) 118087, https://doi.org/10.1016/j.jelechem.2024.118087.
[97] J. Zheng, Y. Wang, In-situ solid-state transformation of MOF-derived hierarchical CoxNi1-xS2 microspheres for high-performance supercapacitors, Mater. Today Commun. 49 (2025) 113877, https://doi.org/10.1016/j.mtcomm.2025.113877.
[98] A.A. Kulkarni, N.K. Gaikwad, A.P. Salunkhe, R.M. Dahotre, T.S. Bhat, Transition metal phosphates: a paradigm for electrochemical supercapacitors, J. Electroanal. Chem. 948 (2023) 117795, https://doi.org/10.1016/j.jelechem.2023.117795.
[99] H. Zhang, Y. Wang, C. Chen, X. Wu, Metal-organic frameworks derived transition metal phosphide/carbon for high performance asymmetric supercapacitor, J. Energy Storage 55 (2022) 105623, https://doi.org/10.1016/j.est.2022.105623.
[100] J. Dai, Z. Li, R. Yu, H. Su, Q. Wang, MOF-derived hollow NiCoP combined with rGO for high-performance hybrid supercapacitors, Ionics 29 (2023) 721–732, https://doi.org/10.1007/s11581-022-04841-8.
[101] A.M. Kale, R. Velayutham, A.D. Savariraj, M. Demir, B.C. Kim, Unravelling the influence of interfacial tailoring in metal-organic framework-derived ultrathin sheets of Co2P/Cu3P for high-performance hybrid supercapacitor, Mater. Today Sustain. 21 (2023) 100335, https://doi.org/10.1016/j.mtsust.2023.100335.
[102] Y. Cui, L. Zhao, D. He, J. Sun, J. Yang, W. Tang, H. Yu, C. Lou, W. Wang, X. Zhang, H. Zhao, Preparation of zirconium-based MOF-Derived phosphide on GO/MXene double substrates for high-performance asymmetric supercapacitors, ACS Appl. Mater. Interfaces 16 (2024) 47751–47762, https://doi.org/10.1021/acsami.4c10803.
[103] C. Wang, J. Kim, J. Tang, M. Kim, H. Lim, V. Malgras, J. You, Q. Xu, J. Li, Y. Yamauchi, New strategies for novel MOF-Derived carbon materials based on nanoarchitectures, Chem 6 (2020) 19–40, https://doi.org/10.1016/j.chempr.2019.09.005.
[104] W. Yang, X. Li, Y. Li, R. Zhu, H. Pang, Applications of Metal–Organic-Framework-Derived carbon materials, Adv. Mater. 31 (2019) 1–35, https://doi.org/10.1002/adma.201804740.
[105] D. Huang, L. Chen, L. Yue, F. Yang, H. Guo, W. Yang, Nitrogen-doped carbon-enriched MOF and derived hierarchical carbons as electrode for excellent asymmetric aqueous supercapacitor, J. Alloys Compd. 867 (2021) 158764, https://doi.org/10.1016/j.jallcom.2021.158764.
[106] R. Andavar, F. Cai, I. Shahid, U.A. Kolachi, Y. Sun, J. Pan, Tailoring pore structure and surface chemistry of bi-metallic MOF-derived porous carbon nanorods for high-performance supercapacitors and sodium-ion batteries, Carbon N. Y. 244 (2025) 120743, https://doi.org/10.1016/j.carbon.2025.120743.
[107] M. He, J. Qiao, B. Zhou, S. Guo, G. Zhu, J. Wang, G.J.H. Melvin, M. Wang, H. Ogata, Y.A. Kim, M. Terrones, M. Endo, F. Zhang, Z. Wang, MOF-derived carbon nanotube/vertical graphene composite: a binder-free electrode for high-performance supercapacitors with aqueous redox electrolyte, Carbon N. Y. 241 (2025) 120415, https://doi.org/10.1016/j.carbon.2025.120415.
[108] R. Miao, C. Sun, J. Li, Y. Sun, Y. Chen, J. Pan, Y. Tang, P. Wan, A facile morphology tunable strategy of Zn-MOF derived hierarchically carbon materials with enhanced supercapacitive performance through the solvent effect, Dalton Trans. 51 (2022) 18213–18223, https://doi.org/10.1039/d2dt02624d.
[109] G. Jiang, S. Osman, R.A. Senthil, Y. Sun, X. Tan, J. Pan, Hierarchically porous carbon derived from magnesium-based metal-organic frameworks as advanced active material for supercapacitor, J. Energy Storage 49 (2022) 104071, https://doi.org/10.1016/j.est.2022.104071.
[110] J. Pokharel, A. Gurung, A. Baniya, W. He, K. Chen, R. Pathak, B.S. Lamsal, N. Ghimire, Y. Zhou, MOF-derived hierarchical carbon network as an extremely-high-performance supercapacitor electrode, Electrochim. Acta 394 (2021) 139058, https://doi.org/10.1016/j.electacta.2021.139058.
[111] J. Park, D. Kim, S. Kim, J. Park, D. Yeol Ryu, J. Kim, H. An, J. Kim, Controlled growth of redox-active polymer nanorods on MOF-derived activated nanoporous carbons: 3D reconstruction study and high-performance supercapacitor, Chem. Eng. J. 498 (2024) 155122, https://doi.org/10.1016/j.cej.2024.155122.
[112] N. Cao, X. Zhang, Q. Li, X. Liu, X. Ma, G. Liu, X. Tang, C. Li, X. Zang, Q. Shao, The role of nitrogen-doping on the electrochemical behavior of MOF-derived carbons in ionic liquid electrolytes, Diam. Relat. Mater. 139 (2023) 110412, https://doi.org/10.1016/j.diamond.2023.110412.
[113] C. Qu, L. Zhang, W. Meng, Z. Liang, B. Zhu, D. Dang, S. Dai, B. Zhao, H. Tabassum, S. Gao, H. Zhang, W. Guo, R. Zhao, X. Huang, M. Liu, R. Zou, MOF-derived α-NiS Nanorods on Graphene as an Electrode for high-energy-density Supercapacitors, 2018, pp. 4003–4012, https://doi.org/10.1039/c7ta11100b.

[114] M. He, J. Qiao, B. Zhou, J. Wang, S. Guo, G. Jet, H. Melvin, M. Wang, H. Ogata, Y. A. Kim, M. Tanemura, S. Wang, M. Terrones, M. Endo, F. Zhang, Z. Wang, Controllable Metal – Organic Framework-Derived NiCo-Layered Double Hydroxide Nanosheets on Vertical Graphene as Mott – Schottky Heterostructure for High- Performance Hybrid Supercapacitor, 2024 2400207, https://doi.org/10.1002/sstr.202400207.

[115] E. Torabi, A. Kazemi, M. Tamtaji, F. Manteghi, S. Rohani, W.A. Goddard, Heliyon Sacrificial MOF-derived MnNi hydroxide for high energy storage supercapacitor electrodes via DFT-based quantum capacitance study, Heliyon 11 (2025) e41261, https://doi.org/10.1016/j.heliyon.2024.e41261.

[116] C. Yang, S. Yun, J. Shi, M. Sun, N. Zafar, A. Arshad, Tailoring the supercapacitive behaviors of Co/Zn-ZIF derived nanoporous carbon via incorporating transition metal species : a hybrid experimental-computational exploration, Chem. Eng. J. 419 (2021) 129636, https://doi.org/10.1016/j.cej.2021.129636.

[117] N. Nwaji, J. Gwak, M. Goddati, H. Kang, A.H. Pasanaje, Defect-Engineered Fe3C@NiCo2S4 nanospike derived from metal-organic frameworks as an, Advanced Electrode Material for Hybrid Supercapacitors (2023), https://doi.org/10.1021/acsami.3c04635.

[118] W. Ning, S. Xu, P. Wang, H. Ma, X. Yang, X. Sun, C. Yang, X. Shi, MOF derived tri-metallic CoNiMn hydroxide assembled on carbon cloth for hybrid supercapacitor and hydrogen evolution, J. Energy Storage 96 (2024) 112758, https://doi.org/10.1016/j.est.2024.112758.

[119] C.J. Balhatchet, J.W. Gittins, S.J. Shin, K. Ge, X. Liu, T. Trisukhon, S. Sharma, T. Kress, P.L. Taberna, P. Simon, A. Walsh, A.C. Forse, Revealing ion adsorption and charging mechanisms in layered metal-organic framework supercapacitors with solid-state nuclear magnetic resonance, J. Am. Chem. Soc. 146 (2024) 23171–23181, https://doi.org/10.1021/jacs.4c05330.

[120] M.R. Lukatskaya, D. Feng, S.M. Bak, J.W.F. To, X.Q. Yang, Y. Cui, J.I. Feldblyum, Z. Bao, Understanding the mechanism of high capacitance in nickel hexaaminobenzene-based conductive metal-organic frameworks in aqueous electrolytes, ACS Nano 14 (2020) 15919–15925, https://doi.org/10.1021/acsnano.0c07292.

[121] W. Zheng, M. Liu, L.Y.S. Lee, Electrochemical instability of metal-organic frameworks: in situ spectroelectrochemical investigation of the real active sites, ACS Catal. 10 (2020) 81–92, https://doi.org/10.1021/acscatal.9b03790.

[122] X.Z. Hongna Xing, Yibo Liu, Xia Deng, Xiao Chi, Yan Zong, Juan Feng, Xiuhong Zhu, Xinghua Li, Hongyang Zhao, In situ observation Zn volatilization and microstructural resolution in ZIF-8 derived porous carbon for supercapacitors, Nano Res. (2026), https://doi.org/10.26599/NR.2026.94908497.

[123] M. Rubio-Martinez, C. Avci-Camur, A.W. Thornton, I. Imaz, D. Maspoch, M. R. Hill, New synthetic routes towards MOF production at scale, Chem. Soc. Rev. 46 (2017) 3453–3480, https://doi.org/10.1039/c7cs00109f.

[124] A. Carné-Sánchez, I. Imaz, M. Cano-Sarabia, D. Maspoch, A spray-drying strategy for synthesis of nanoscale metal-organic frameworks and their assembly into hollow superstructures, Nat. Chem. 5 (2013) 203–211, https://doi.org/10.1038/nchem.1569.

[125] D. Crawford, J. Casaban, R. Haydon, N. Giri, T. McNally, S.L. James, Synthesis by extrusion: continuous, large-scale preparation of MOFs using little or no solvent, Chem. Sci. 6 (2015) 1645–1649, https://doi.org/10.1039/c4sc03217a.

[126] J. Klinowski, F.A. Almeida Paz, P. Silva, J. Rocha, Microwave-Assisted synthesis of metal–organic frameworks, J. Chem. Soc., Dalton Trans. 40 (2011) 321–330, https://doi.org/10.1039/c0dt00708k.

[127] U. Mueller, M. Schubert, F. Teich, H. Puetter, K. Schierle-Arndt, J. Pastré, Metal-organic frameworks-prospective industrial applications, J. Mater. Chem. (2006) 626–636, https://doi.org/10.1039/b511962f.